Atmospheric H_2 observations from the NOAA Cooperative Global ~~Cooperative~~ Air Sampling Network

Gabrielle Pétron[1,2], Andrew M. Crotwell[1,2], John Mund[1,2], Molly Crotwell[1,2], Thomas Mefford[1,2], Kirk Thoning[2], Bradley Hall[2], Duane Kitzis[1,2], Monica Madronich[1,2], Eric Moglia[1,2], Donald Neff[1,2], Sonja Wolter[1,2], Armin Jordan[3], Paul Krummel[4], Ray Langenfelds[4], John Patterson[5]

Correspondence to: Gabrielle Pétron (gabrielle.petron@noaa.gov)

1. Cooperative Institute for Research in Environmental Sciences, CU Boulder, USA
2. NOAA Global Monitoring Laboratory, Boulder, USA
3. Max-Planck-Institute for Biogeochemistry (MPI-BGC), Jena, Germany
4. Commonwealth Scientific and Industrial Research Organisation - Environment, Aspendale, Australia
5. Department of Earth System Science, University of California, Irvine, USA

Abstract. The NOAA Global Monitoring Laboratory (GML) measures atmospheric hydrogen (H_2) in grab-samples collected weekly as flask pairs at over 50 sites in the Cooperative Global Air Sampling Network. ~~These NOAA H_2 measurements from 2009 to 2021 are publicly available.~~ Measurements representative of background air sampling show higher H_2 in recent years at all latitudes. The marine boundary layer (MBL) global mean H_2 was 552.8 ppb in 2021, 20.2 ±0.2 ppb higher ~~in 2021~~ compared to 2010. A 10 ppb or more increase over the 2010-2021 average annual cycle was detected in 2016 for MBL zonal means in the tropics and in the Southern Hemisphere. Carbon monoxide measurements in the same air samples suggest large biomass burning events in different regions likely contributed to the observed interannual variability at different latitudes. The NOAA H_2 measurements from 2009 to 2021 are now based on the ~~A major focus in recent years involved the adoption of~~ the World Meteorological Organization Global Atmospheric Watch (WMO GAW) H_2 mole fraction ~~X2009~~ calibration scale, developed and maintained by the Max-Planck Institute for Biogeochemistry (MPI-BGC), Jena, Germany. GML maintains eight H_2 primary calibration standards to propagate the WMO~~MPI~~ scale. These are gravimetric hydrogen-in-air mixtures in electropolished stainless steel cylinders (Essex Industries, S~~s~~t. Louis, MO), which are stable for H_2. These mixtures were calibrated at the MPI-BGC, the WMO Central Calibration Laboratory (CCL) for H_2, in late 2020 and span the range 250-700 ppb. We have used the CCL assignments to propagate the WMO~~MPI X2009~~ H_2 calibration scale to NOAA air measurements performed using Gas Chromatography-Helium Pulse Discharge Detector instruments since 2009. To propagate the scale, NOAA uses a hierarchy of secondary and tertiary standards, which consist of high-pressure whole air mixtures in aluminum cylinders, calibrated against the primary and secondary standards respectively. Hydrogen at the ppb-level has a tendency to increase in aluminum cylinders over time. ~~To propagate the scale, NOAA uses a hierarchy of secondary and tertiary standards, which are high pressure tanks with whole air mixtures calibrated against the primary and secondary standards respectively. NOAA secondary and tertiary standards are stored in aluminum cylinders, which have a tendency to grow H_2 over time.~~ We fit the calibration histories of these standards with 0-2nd order polynomial functions of time and use the time-dependent mole fraction assignments on the ~~MPI X2009~~ WMO scale to reprocess all tank air and flask air H_2 measurement records. The robustness of the scale propagation over multiple years is evaluated with the regular analysis of target air cylinders and with long-term same air measurement comparison efforts with WMO GAW partner laboratories. Long-term

calibrated, globally distributed and freely accessible measurements of H_2 and other gases and isotopes continue to be essential to track and interpret regional and global changes in the atmosphere composition. The adoption of the WMOMPI X2009 H_2 calibration scale and subsequent reprocessing of NOAA atmospheric data constitute a significant improvement in the NOAA H_2 measurement records.

1 Introduction

High quality and sustained observations are essential to track and study changes in atmospheric trace gas distributions. Ambient air measurement programs for trace gases provide objective data to track air pollution levels [Oltmans and Levy, 1994; Thomson et al., 2004; Tørseth et al., 2012; Schultz et al., 2015; Cooper et al., 2020; WMO, 2022], to study how a mix of sources (and sinks) impact the air composition [Ciais et al., 1995; Pétron et al., 2012; Langenfelds et al., 2002; Brito et al., 2015] and to constrain and evaluate fluxes and their trends at scales of interest [von Schneidemesser et al., 2010; Simpson et al., 2012; Propper et al., 2015; Montzka et al., 2018; Friedlingstein, 2022; Heiskanen et al., 2022; Storm et al., 2023] at scales of interest.

H_2 is a trace gas in the Earth's atmosphere and its abundance can indirectly impact climate and air quality. The analysis of H_2 measurements in firn air collected in Antarctica reveal that H_2 levels in the high-latitude southern hemisphere grew by some 70% (330 to 550 ppb, 1 ppb = 1 mole of gas per billion (10^9) moles of air) over the 20th century [Patterson et al., 2021; 2023]. Greenland firn air covers less depth and time but results are consistent with a 30% increase in high-latitude northern hemisphere H_2 from 1950 to the late 1980s [Patterson et al., 2023]. Growing emissions related to fossil fuel burning most likely were behind this rise in H_2 [Patterson et al., 2021]. Results also show that H_2 in both polar regions leveled off after the 1990s [Patterson et al., 2021, 2023].

H_2 has been viewed as a potential low or zero carbon energy carrier for close to five decades [Yap and McLellan, 2023]. Since 2020 there has been renewed interest in the hydrogen economy [Yap and McLellan, 2023] spurred by a rise in announcements of public and private projects to produce low carbon H_2, also referred to as "blue" H_2 produced from natural gas with carbon capture, utilization and storage, or "green" H_2 produced using renewable energy [Hydrogen Council and McKinsey & Company, 2023]. In 2021, H_2 global demand was over 94 million tonnes or 2.5 % of global final energy consumption [IEA, 2022]. This demand was almost entirely driven by refineries and a few industries (ammonia, methanol and steel) and H_2 production almost entirely relied on fossil fuels with unabated emissions ("gray H_2", [IEA, 2022]). As of December 2023, over 1,400 announced projects globally (worth US$ 570 billion) are anticipated to increase the global H_2 production capacity by 45 million tonnes through 2030 [Hydrogen Council and McKinsey & Company, 2023].

Studies of the potential short-term and long-term climate impacts of increased H_2 production and use have called for more research to better understand the current and future H_2 supply chain and end-use emissions of H_2 and GHGs [Ocko and Hamburg, 2022; Longden et al., 2022; de Kleijne et al., 2022; Bertagni et al., 2022; Warwick et al., 2023]. Global, high quality and sustained atmospheric measurements of H_2 can provide independent information to document its distribution and study its sources and sinks and how they may change.

The National Oceanic and Atmospheric Administration (NOAA) Cooperative Global Air Sampling Network comprises over 50 surface and mostly remote sites (https://gml.noaa.gov/ccgg/flask.html). At each site and on a weekly basis, local partners collect air in two 2.5-L glass flasks, and then return the flasks to the NOAA Global Monitoring Laboratory (GML) in Boulder, Colorado, USA, for measurements of major long-lived greenhouse gases, carbon dioxide (CO_2), methane (CH_4), nitrous oxide (N_2O), sulfur hexafluoride (SF_6), as well as carbon monoxide (CO) and hydrogen (H_2) [Conway et al., 1994; Novelli et al., 1999; Dlugokencky et al., 2009]. The network is a contributor to the World Meteorological Organization (WMO) Global Atmospheric Watch (GAW) Programme, which promotes and coordinates international scientific efforts and free access to long-term atmospheric observations [WMO, 2022].

CO and H_2 are important trace gases that share sources with CO_2 and CH_4 (fossil fuel burning, biofuel burning and wildfires). Reaction with hydroxyl radicals (OH) is the main sink for CH_4 and CO and an important sink for H_2. Both H_2 and CO are also produced during the chemical oxidation of CH_4 and nonmethane hydrocarbons. Soil uptake by bacteria accounts for 75% of the total H_2 sink. H_2 and CO have much shorter atmospheric lifetimes than CO_2 and CH_4: 2-3 months for CO and close to 2 years for H_2. The H_2 global mean atmospheric lifetime is largely driven by the soil sink strength. The H_2 lifetime related to the oxidation by OH is estimated to be 8-9 years [Price et al., 2007; Warwick et al., 2022].

~~The "Geophysical Monitoring for Climatic Change" was the original program established by NOAA to gather and analyze observations of the background atmosphere composition. GMCC started measuring CO_2 in background air samples in 1968 [Komhyr et al., 1985]. CH_4 was added in 1983 [Steele et al., 1987]. In the late 1980s, GMCC and its successor the Climate Monitoring and Diagnostics Laboratory expanded operations to measure CO in the global network air samples to add a constraint for the study of combustion sources and the global carbon budget. The analytical instrument selected consisted of a gas chromatograph (GC) and a reduction gas analyzer (RGA, from Trace Analytical Inc., California) that could measure both CO and H_2. ¶~~

Novelli et al. [1991~~2~~, 1992~~1~~] ~~first~~ reported for NOAA on testing the air sampling approach (flask type, stopcock fitting, wet/dry air, untaped versus taped glass flasks to minimize direct sunlight exposure) and an analytical instrument consisting of a gas chromatograph (GC) and a reduction gas analyzer (RGA, from Trace Analytical Inc., California)~~GC-RGA instrumentation~~ that could measure both CO and H_2~~for CO~~. Around that time, other laboratories had also adopted the ~~GC-RGA measurement~~ technique for CO and H_2 measurements in discrete air samples or in situ. Khalil and Rasmussen [1989, 1990] reported on H_2 measurements of whole air samples collected weekly in triplicate electropolished stainless steel flasks between October 1985 and April 1989 at the four NOAA atmospheric baseline observatories (Point Barrow, Mauna Loa, Samoa, South Pole), Cape Meares, Oregon, Cape Kumukahi, Hawaii and at the Cape Grim Observatory, Tasmania. These measurements showed that, contrary to CO_2, CH_4, N_2O and CO, background air H_2 levels were higher in the Southern Hemisphere (SH) than in the Northern Hemisphere (NH). 1985-1987 monthly mean observed H_2 ranged between 500-520 ppb at the South Pole and between 455 and 520 ppb at Point Barrow. H_2 exhibited a strong seasonal cycle at extratropical latitudes especially in the NH and the seasonal cycles in both hemispheres were offset by 1-2 months only.

In 1995, H_2 mole fraction calibration standards were prepared gravimetrically in aluminum~~Scott Marrin Inc.~~ cylinders (Scott Marrin Inc., Riverside, CA) and five of them (spanning 485-603 ppb) were used to define the NOAA H_2 X1996 calibration scale. Working standards used in the NOAA flask analysis laboratory between 1988 and 1996 were reassigned H_2 mole fractions and flask air measurements were reprocessed to be on the X1996 scale. Novelli et al. [1999] described the early NOAA H_2 measurements and reported H_2 time series starting in the late 1980s or early 1990s (depending on the site) for 50 sites in the NOAA Cooperative Global Air Sampling Network.

Simmonds et al. [2000] reported in-situ high-frequency GC-RGA3 measurements of H_2 at the Mace Head baseline atmospheric monitoring station on the Atlantic coast of Ireland for the 1994-1998 period. They found that the background air at Mace Head had lower monthly mean H_2 (470-520 ppb) than background air masses measured at the Cape Grim observatory (510-530 ppb) from July to April. Some of the 40 min H_2 observations showed 10~~s~~-200 ppb short-term H_2 enhancements above baseline levels. The authors derived an estimate of European emissions with an inverse model of enhanced H_2 in air masses impacted by upwind sources of pollution. They also observed that nighttime measurements in low wind conditions reflected local depletion of H_2. The authors derived variable mean deposition velocities and found that the H_2 soil sink was likely a process that occurred year-round in the area.

After 1996 and until 2008, the NOAA H_2 measurement program used successive working standards that were assigned based on GC-RGA measurements against the previous standards. With hindsight, the NOAA X1996 calibration scale transfer and the early NOAA H_2 measurements had several limitations which are briefly described below and in more detail in the Supplementary Information section S1.

By the late 1990s, same air or collocated air sample measurement comparison between NOAA and the Commonwealth Scientific and Industrial Research Organisation (CSIRO) for the Cape Grim Observatory and Alert, Canada, flask air analyses showed an increasing bias for H_2 between the two laboratories [Masarie et al., 2001; Francey et al., 2003]. Further laboratory tests by several WMO/GAW measurement laboratories revealed the RGA detector response was non linear and required frequent calibration. Additionally measurement laboratories found that the H_2 mole fraction for air standards, especially those stored in high pressure aluminum cylinders, could drift at rates of a few parts per billion (ppb) to tens of ppb~~s~~ per year [Novelli et al., 1999; Masarie et al., 2001; Jordan and Steinberg, 2011].

To address these compounding issues, in 2008 NOAA GML tested a new analytical instrument: a gas chromatograph with a pulse discharge helium ionization detector (GC-HePDD) [Wentworth et al., 1994]. The technique showed very good performance with a stable and linear response over the 0-2000 ppb range and it was adopted for the calibration scale propagation and flask air analysis in 2009 [Novelli et al., 2009]. Around that time GML~~NOAA~~ also began testing electropolished stainless steel cylinders (Essex Industries, St. Louis, MO) filled with dry air for stability.

In 2007-2008, GML prepared six new gravimetric air mixtures in electropolished stainless steel cylinders spanning 250-600 ppb H_2. At that time, the new gravimetric mixtures differed by about +20 ppb compared to two H_2 secondary standards values assigned on the NOAA H_2 X1996 scale. For the next decade, GML kept using the NOAA X1996 calibration scale while also conducting routine measurements of the H_2 secondary standards against the 2007/2008 gravimetric mixtures.

The GC-HePDD H_2 measurements on the NOAA H_2 X1996 scale remained biased compared to GAW partner measurements and the NOAA H_2 data from the global network flasks were not released publicly after 2005. SI sections S1-3 and SI Table 1 provide additional background information on issues impacting the 1988-2008 NOAA H_2 measurements on RGAs, and related information from the CSIRO and Max-Planck Institute for Biogeochemistry (MPI-BGC) H_2 measurement programs. The best more precise and better calibrated NOAA H_2 measurement records date back to 2009/2010 and are the main focus of this paper.

In Fall 2020, GML initiated an effort to 1) adopt the WMO MPI X2009 H_2 calibration scale [Jordan and Steinberg, 2011] for future measurements and 2) convert GML H_2 measurements made on GC-HePDD instruments (beginning in late 2009) to that scale. This paper describes the MPI X2009 H_2 calibration scale propagation within GML and the revised measurements from the NOAA Cooperative Global Air Sampling Network flask air samples analyzed since late 2009. We show very good agreement for the reprocessed NOAA H_2 data for different WMO/GAW measurement comparison efforts. The revised NOAA GML flask air H_2 dry air mole fraction measurement records for 70 surface sites from 2009-2021 are publicly available [Pétron et al., 2023a]. This new dataset complements other WMO/GAW H_2 measurement datasets and provides reliable observational constraints for the study of atmospheric H_2 global distribution and budget since 2009. Future NOAA H_2 dataset updates will be released as we use continued calibration results to reliably track the drift in working standards and revise their assignments.

2 Adoption of the WMO MPI X2009 H_2 calibration scale

To infer fluxes and trends from atmospheric measurements, scientists need to reliably detect small temporal and spatial gradients in the abundance of trace gases. This requires comparable data across time and across monitoring networks to ensure biases are minimized and do not influence interpretation. The use of a common calibration scale among measurement laboratories ensures data are traceable to a common reference. It is the first step in preventing biases that could stem from using different references.

In this section, we introduce the NOAA GML H_2 calibration standard hierarchy and describe the adoption of the WMO MPI X2009 H_2 scale. First we introduce the GML H_2 primary standards. Calibration at GML is based on a hierarchy of standards (primary, secondary, tertiary, etc.) primary standards and Then we describe the GML tank air and a dedicated H_2 calibration system used to transfer the scale and the scale transfer from the primary standards to secondary and tertiary standards (2009-April 2019) or from the primary standards to secondaryworking standards (after April 2019). The tertiary standards (until April 2019) and secondaryworking standards (after April 2019) are used to calibrate the H_2 instrument response on the flask air analysis systems and value assign discrete air measurements. An important quality assurance procedure within GML is the routine measurement of dedicated quality control cylinders (referred to as "Target" tanks) to track instrument performance. Results are discussed in relation to the uncertainty of the flask air analysis systems and consistency of the MPI X2009 H_2 scale implementation.

2.1 NOAA GML H_2 primary standards

In 2007-2008, six mixtures of H_2 in dry air air mixtures spanning a range of H_2 dry air mole fractions were prepared gravimetrically at GML in electropolished stainless steel 34L cylinders ([Novelli et al., 2009], and Table 1). The highest H_2 mole fraction tank developed a leak and was lost. The remaining set of five standards covered the range 250 ppb to 600 ppb for H_2. Three standards in electropolished stainless steel cylinders were added in 2019 to extend the upper limit of the calibration range to 700 ppb H_2 and evaluate the stability of the initial set over the intervening years. In 2020, t~~T~~hese eight standards were~~have been~~ designated ~~by GML~~ as NOAA GML's~~our~~ highest level H_2 standards. We refer to them as the NOAA H_2 primary standards throughout this document even though they are not used to independently define ~~are not defining~~ the scale.

The eight primary standards were analyzed by the WMO Central Calibration Laboratory (CCL) for H_2 hosted by the MPI-BGC in Jena, Germany, on their GC-PDD system in November 2020. The results listed in Table 1 are reported on the MPI X2009 H_2 calibration scale [Jordan and Steinberg, 2011]. The CCL uncertainty estimates listed in Table 1 refer to the standard deviation of the 25-32 discre~~e~~te H_2 measurements made for each standard. Until they are recalibrated by the CCL, we add an 0.5 ppb 1-sigma uncertainty to these assignments. This is the currently reported CCL reproducibility for their GC-~~He~~PDD H_2 measurements. It accounts for potential longer term uncertainty in calibration results that would not be evident in the standard deviations of measurements made close in time.

2.2 MPI X2009 H_2 calibration scale transfer

GML has separate, dedicated analytical systems for scale propagation and flask air analyses. Novelli et al. [2009] describe the GC-HePDD instruments and the operating parameters in detail. GML has used three GC-HePDD instruments so far. Each is identified by a unique internal instrument identification code: H9 ~~(Agilent 6890 GC, serial number US10326037)~~ for tank calibrations and H8 ~~(Agilent 6890 GC, serial number US10326011)~~ and H11 ~~(Agilent 7890 GC, serial number US10834030)~~ for flask analyses. The GC-HePDD instruments' responses are linear (within 0.3%) up to 2000 ppb. They are configured for ppb level sensitivity and calibrated over the 200-700 ppb range, which is optimal for global and regional background air analysis.

The GML H_2 primary standards are used to periodically calibrate the H9 instrument response for the analysis and value assignment of lower level standards. ~~GML used secondary standards from 2009 through April 2019 in the calibration hierarchy but has since removed this level to reduce the number of standards which can potentially drift (see discussion of drifting cylinders later in this document).~~ The stability and longevity of the primary standards are critical to ensure the consistency of the GML H_2 measurements over long periods of time as required for trend analysis.

The H_2 secondary and tertiary ~~(or working)~~ standards~~)~~ used in GML are whole air mixtures in high pressure aluminum cylinders (Luxfer USA). Most were filled at the GML standard air preparation facility at the Niwot Ridge mountain research station using a Rix Industries (Benicia, CA) SA6 oil-free compressor [Kitzis, 2017]. Two additional tertiary standards ~~(CB11551 and CC305198)~~ were purchased from Scott Marrin. All GML tank air mixtures have a unique combination of an alphanumeric cylinder ID and a fill code letter (A-Z) tied to a fill date.

Aluminum tanks are known to be unstable for storing H_2 in air standards [Jordan and Steinberg, 2011]. Therefore regular analyses of ~~working~~ standards on the tank calibration~~s~~ system are critical for quantifying drift to allow a time dependent value assignment on the MPI X2009 H_2 calibration scale.

~~The calibration history for a secondary, tertiary or working standard only uses retained (valid) calibration event results on H9.~~ GML uses python software developed in-house~~in house~~ to record calibration data, compute mole fractions, and ~~write instrument output files and to calculate a calibration event result. Another piece of python code is used to analyze tank air calibration histories and~~ evaluate ~~if~~ the stability of H_2 mole fractions ~~in the tank is stable or if it changes~~ over time. ~~For many GML H_2 calibration standards and target air tanks, a linear or quadratic function is the best fit through their calibration history. When this happens, the function coefficients define the tank time-dependent assignment.~~ All mole fraction assignments and associated drift coefficients for standards used to propagate a calibration scale are stored in a database table that can be accessed by the data processing software. The software allows for 0-2nd order~~linear and~~ polynomial drift functions. As new calibration results are available, the drift correction and assignment for a particular tank ID and fill code are~~is~~ revised as needed and the affected data are~~is~~ reprocessed.

2.2.1 Scale transfer~~Tank calibration system~~: 2009-2019 ~~configuration~~

From 2007 through mid-April 2019, the H_2 tank air calibration on the H9 instrument was conducted using a single standard gas (primary or secondary standard) to calibrate the "unknown" (secondary or tertiary) standards. A tank~~Each~~ calibration event consisted of alternating injections of the reference/standard gas and the "unknown" tank air with typically seven or more unknown air injections. The first aliquot in a multi injection measurement sequence on H9 is often slightly biased (due to subtle timing differences with the regulator flush cycle) and is not used. The ratio of the H_2 peak height for each valid "unknown" air injection and the mean peak height of two bracketing reference gas injections (or sometimes only one preceding or following reference gas injection) is multiplied by the reference/standard gas known H_2 mole fraction to calculate the "unknown" air injection mole fraction. Results for a tank air calibration event are defined by the mean and the standard deviation of the calculated H_2 mole fractions for five or more retained unknown air injections. Typically, the standard deviation for a tank air calibration event on H9 is less than 1 ppb.

Prior to the 2023 GML H_2 data reprocessing, GML used peak area for the GC-HePDD as described in Novelli et al. [1999]. However, we saw that for some Helium carrier gas tanks (Airgas Ultra High Purity, (99.999% purity), the H_2 chromatogram peak had a tail or a noisy baseline. Since the H_2 peak height was less affected, we use peak height ratios for all GC-HePDD measurements. In 2023, GML switched to Matheson Research Grade Helium carrier gas for the GC-HePDDs (99.9999% purity).

~~Two secondary standards with background ambient air level H_2 were in service on H9 to calibrate tertiary standards: CC119811 (2008/02 to 2013/06) and CA03233 (2013/06 to 2018/11). These two standards were calibrated periodically on H9 against individual members of the primary standard suite. Most calibration episodes consisted of one to 6 calibration sequences over 1-3 successive days, each against one of the primary standards. For CC119811, 1-point calibration sequence results in 2008, 2009, 2010 and 2013 against one of the two lowest primary standards (SX-3558 and SX-3543) show a 3 to 5 ppb positive~~

~~bias which suggests a small non zero intercept in the instrument response during those times. This primary standard dependent bias is not apparent for CA03233 results between 2014 and 2016. Results against SX-3558 were not used for value assigning either secondary standards and results against SX-3543 were not used for CC119811.~~

The calibration results for the two H_2 secondary standards used between 2009 and Arpil 2019 are plotted in Figure 1 and final assignments are listed in SI Table 2. A small non zero y-intercept for H9 (see next section) likely explains the biased results for CC119811 against the lowest primary standards (SX-3558 and SX-3543). Results against SX-3558 were not used for value assigning either secondary standards and results against SX-3543 were not used for CC119811.

CA03233 was stable for H_2 over its time of use and has an assignment of 502.8 ppb H_2. H_2 in CC119811 exhibited a small linear drift and its value assignment is time dependent with a growth rate of 2 ppb/yr. Between 2009 and 2019, these two secondary standards were used on H9 to calibrate seventeen H_2 tertiary standards used in the NOAA flask~~discrete air sample~~ analysis laboratory.

2.2.2 Scale transfer~~Tank air calibration system~~ ~~configuration~~: 2019-present ~~configuration~~¶

Beginning in April 2019, GML transitioned H9 to use a multi-point calibration strategy to better define the instrument response. The eight H_2 primary standards are measured relative to a reference air tank (CC49559, filled with~~at~~ ambient Niwot Ridge dried air) to calibrate the instrument response. A multi-standard response calibration episode for H9 involves the alternating injections from the reference air tank and each primary standard. Each standard is injected 8 times alternating with reference air aliquots. The entire response calibration sequence takes close to 15 hours. GML has performed an H9 instrument response calibration 2 to 3 a few times a year, followed by tank calibrations ~~2 to 3 a few times a year~~ over a 10-14 day period each time.

The H9 instrument response function is calculated as the best linear fit to the primary standards' mean normalized chromatogram peak heights and their CCL H_2 mole fraction assignments. H9 calibration curves are assumed to be valid for several weeks during which time other air cylinders are analyzed relative to the same reference tank.

Between April 2019 and December 2022, the H9 instrument response was determined relative to the primary standards ~~calibrated~~ nine times. Figure 2a shows the deviations of the H9 linear response functions from the line defined by computing the mean value for the intercept and slope of the 2019-2022 response functions. The instrument response has remained stable within +/- 1 ppb over this time period over the range 200-700 ppb. ~~Figure 2b shows the residuals to the best linear fit for each instrument response calibration episode. We note that the H9 instrument response has been quite stable over the 200-700 ppb range but that the linear fit does not go through the origin.~~ The residuals to each~~the~~ linear fit over this time period are all within the -0.6 ppb to 0.5 ppb range (Figure 2b). The linear fit y-intercept ranges between 3.9 and 5.5 ppb (not shown). Prior to 2019, we assumed a zero intercept for the H9 one point calibration. If we assume a y-intercept around 5 ppb was more likely, it is possible the pre-2019 H9 measurements (with 1 point calibration) were biased by ~1% of the difference between the tank air and the reference/standard H_2 mole fractions. We do not correct for this potential bias at this time.

Since April 2019,~~A~~ a tank air calibration~~measurement~~ sequence on H9 has~~typically~~ consisted~~s~~ of 7 tank air injections, each bracketed by reference air injections. The peak heights for the first injections of reference air and tank air ~~on H9~~ can have a small low bias and are not used. The normalized peak heights for the valid tank air injections are converted to H_2 mole fractions using the most recent H9 ~~instrument~~ response function~~calibration episode~~. The average and standard deviation of the retained injection H_2 mole fractions are stored in a database table.

2.2.3 H_2 standards and calibration approach for the flask air analysis system

~~The NOAA Global Cooperative Air Sampling Network dates back to 1967. In recent years, it has included over 50 surface sites distributed around the world (https://gml.noaa.gov/ccgg/behind_the_scenes/network.html). Partners at each site collect air sample pairs in two 2.5L glass flasks filled simultaneously once a week and return the samples to NOAA GML in Boulder.~~ H_2 in ~~those~~ flask air samples is measured in addition to long-lived GHGs (CO_2, CH_4, N_2O, SF_6) and CO by the Measurement of Atmospheric Gases that Influence Climate Change (MAGICC) system in the NOAA GML Boulder laboratory. Until mid 2019, GML operated two nearly-identical automated flask air analytical systems: MAGICC-1 (1997-2019) and MAGICC-2 (2003-2014). Since mid-2019, GML has used a new MAGICC-3 system. This new system improved analytical techniques for CO_2, CH_4, N_2O, and CO but continues to use the same GC-HePDD instruments from the older systems.

Two GC-HePDD instruments have been used for hydrogen analysis on the three flask air analysis systems since 2009: H8 (MAGICC-2: 2009-2014 and MAGICC-3: August 2019-September 2020) and H11 (MAGICC-1: 2010-July 2019 and MAGICC-3: September 2020-present).

On MAGICC-1 and MAGICC-2, the H_2~~He-PDD~~ instrument response was calibrated using a single tertiary standard (measured before and after each sample aliquot), similar to the original 1 point calibration approach used on H9.

Out of 17~~Typically, the~~ H_2 tertiary standards used during that time, 3 were used for more than 14 months ~~14 lasted less than a year~~ and 14~~most~~ displayed H_2 growth over time. Figure 3 shows the calibration histories for H8 and H11 tertiary standards and their start/deployment dates. For each tertiary standard, assigned mole fractions, drift coefficients, and estimated uncertainties are stored in a database (SI Table 2~~sXX~~). ~~2 provides a list of the standard cylinder IDs and fill codes and information for their mole fraction assignments: t0 date, the best polynomial function fit coefficients relative to time t0 (ci, i=0,2) and an estimated 1-sigma uncertainty.~~ The uncertainty reported in SI Table 2 is empirically derived and based on the standard calibration history and the standard deviation of the residuals to the best fit (the assignment). The python code that ~~used to~~ calculates a secondary or~~the~~ tertiary standard assignment uses a 0.5 ppb 1-sigma H9 reproducibility uncertainty which is added in quadrature to the measurement episode standard deviation to account for longer term uncertainties not evident in the standard deviation of the n-aliquots. We do not formally include an uncertainty for the secondary standard assignment. The H9 reproducibility term is based on the mean of the standard deviation of residuals to the fit for the calibration histories of secondary standards and target tanks over the period 2008-2022 (see section 2.3.1).

The 17 ~~number of~~ tertiary standards used successively on the flask analysis~~older~~ systems between 2009 and 2019 introduce~~s~~ time dependent issues due to the variable rate of H_2 drift in aluminum tanks and the ~~frequency of the~~ tank calibration histories~~s on the calibration system~~. Some of the ~~H11~~ tertiary standards only have pre-deployment calibration results which do not assess drift during use ~~(CC71649, CA04505, CC105491)~~ and other standards have calibration results during their time in use but do not have post deployment calibrations that may help us evaluate the drift rate for the last couple of weeks or months of use (SI Table 2, notes in column “N”~~ND46735, ND33801, CB11551, CB11090, CA08107~~). Three~~A few~~ standards exhibited an increased drift rate towards the end of their life that we did not capture with their infrequent calibrations on H9. This change in drift behavior was observed as increasing biases for measurements of target air tanks and daily test air flasks (see section 3.2). We have applied offline mole fraction corrections to the flask air analysis H_2 results to correct for the end of use drift increase for these three tertiary standards~~ CC71649 (H11), CB11551 (H11) and CC305198 (H8)~~, and their~~ standards’~~ assignment uncertainty is larger for these time periods (SI Table 2).

Since August 2019, the~~GML has used a newer analytical system (called~~ MAGICC-3 system operates with~~) in the flask air analysis laboratory with~~ a GC-HePDD ~~(instrument code H8 and later H11)~~ for H_2, new optical analyzers for CO_2, CH_4 (CRDS, Picarro), CO and N_2O (QC-TILDAS, Aerodyne), and a GC-ECD for SF_6. The responses of the instruments ~~on MAGICC-3~~ are calibrated at the same time using a single set of 11 standards spanning a range of mole fractions for the six trace gases. The MAGICC-3 standards were filled at the Niwot Ridge standard air preparation facility on a few different days between December 2017 and May 2018. Their H_2 mole fractions~~y~~ are regularly~~is are regularly~~ measured on H9 against the GML H_2 primary standards.

For the MAGICC-3 instrument response calibration, the eleven standards are analyzed sequentially relative to an uncalibrated reference air tank (filled at Niwot Ridge). Air from each standard is injected 6 times alternating with the reference air. This entire sequence takes close to 17 hours. The first injection of each standard is often biased low by about 2 ppb for H_2 due to timing issues at the start of each standard sequence and only the remaining 5 injections are used to obtain the average normalized peak height “signal” for each standard.

For H_2, a subset of 8 of the 11 MAGICC-3~~working~~ standards are used to determine~~ calibrate~~ the GC-HePDD response. The time-dependent H_2 value assignment for each standard was derived from 8 or 9 calibration events on H9 between June 2018 and December 2022~~, listed in Table 3~~ (SI Table 3, SI Figures 1 and 2). We plan on analyzing the MAGICC-3 standards 2 to 3 times a year going forward. The standards’ H_2 assignments will be revised as needed. The three cylinders that are not used exhibit complex H_2 growth that is not well captured with periodic calibration episodes and a linear or quadratic fit.

The time between MAGICC-3 instrument response calibration sequences was 2 weeks for the first 3 months of service ~~of MAGICC-3~~ and it has been increased to 4-5 weeks as we found the results to be quite stable. A reference air cylinder will last 9 to 12 months on MAGICC-3. When the MAGICC-3 reference air cylinder is changed (pressure close 250 psia), a new instrument response calibration episode is done with the new reference air cylinder before flask air samples are analyzed.

For the asynchronous calibration to stay valid for up to 5 weeks requires the reference gas composition for the six measured gases to be stable between successive calibration episodes~~dates~~. This has been true so far except for one reference air cylinder ~~CA04145~~ for which a small time dependent H_2 correction was applied between two instrument response calibration dates ~~from 2019-11-06 to 2020-01-16~~ (see SI Figure 3 and more details in SI section S4).

2.3 Calibration scale transfer quality assurance

GML target air tanks are dedicated air mixtures used for measurement quality control over multiple years ~~periods~~. Most are high pressure aluminum cylinders filled at the Niwot Ridge standard preparation facility. The analysis of target air helps us evaluate the robustness of the calibration scale transfer, and the consistency of measurements over time and also between different analytical systems. In a perfect program, we should be able to reproduce a measurement result for a target air tank every time. As noted earlier, however, the reality is more complicated as H_2 tends to grow with time in aluminum cylinders. Tracking many aluminum cylinders provides a diverse history of behaviors (stable, or linear vs non-linear drift), and aids in the understanding of similar cylinders used for calibration.

2.3.1 Calibration system (H9) Target air tanks

Some GML target air cylinders are used exclusively to evaluate the stability and performance of the H9 measurements. Other target air cylinders are analyzed on H9 and in the flask air analysis laboratory on the H8 and H11 instruments to evaluate~~understand~~ the scale transfer.

While H_2 has been increasing in most of our target air tanks, eleven H9 target air tanks have shown either stable H_2 or a linear rate of increase less than 1 ppb/yr. Figure 4 shows the calibration histories for these tanks as well as the residuals from the best fit for each tank. Table 2~~1~~ has a list of these target tanks and several others binned by linear drift rate. More details for target tanks ~~and their trend best fit coefficients~~ are in SI Table 4 ~~S1~~. For each bin, the standard deviation of the residuals (differences of the H9 calibration results minus the best fit values) is below 0.5 ppb. The standard deviation of all linearly drifting target tanks residuals binned together is 0.4 ppb.

~~The regular analysis of target tanks on H9 (right after the instrument response has been calibrated against the primary standards) is used to evaluate the robustness of the calibration scale transfer in GML.~~ Results for tanks with stable or very slowly drifting H_2 indicate that between 2008 and 2021, the scale transfer on H9 has low uncertainty (< 1 ppb). ¶

¶

We have eleven other target tanks for which the best fit to their calibration history is a quadratic function (SI Figure 4 and SI Table 4~~S1~~). The standard deviation of these tanks' residuals binned together is 0.7 ppb. The current set of H9 target air tank results show that residuals for higher mole fraction (>650 ppb) tanks have a larger standard deviation (0.5-0.8 ppb, SI Figure 4d).

~~One tank (CC309852 A, fill date 2009-10-01) with a quadratic drift correction is on the lower end of the GML calibration range with a H_2 mole fraction that grew from 204 ppb in 2009 to 232 ppb in 2021. The standard deviation for this target tank residuals is 0.93 ppb. It appears that a quadratic fit does not capture the observed growth very well. If we reject the first calibration result in 2009 and only fit the other 2011-2021 results showing the H_2 mole fraction increasing from 217 ppb to 232 ppb, the best fit is a still a quadratic function but with smaller coefficients (c1 = 1.66 ppb and c2 = -0.16 ppb) and the standard~~

~~deviation of the residuals to this fit is reduced to 0.36 ppb. Similarly, other~~ Some tanks that were analyzed soon after fill and over several years show a ~~similar~~ rapid and large initial growth in H_2 (in the first 0.5-2 years after fill). In this scenario, the residuals to a best linear or quadratic fit of the full calibration history will be larger and will likely not capture the tank time-dependent H_2 assignment as accurately. For a few of the GML standard and target air tanks, we dropped early calibration results that would bias the best fit derivation and assignment during the time of use of the tank.

2.3.2 Comparison of measurements of gas mixtures in cylinders with MPI-BGC

Since 2016, the MPI-BGC GasLab has organized same tank air measurement ("MENI") comparisons between WMO GAW partner laboratories as part of the European ICOS (Integrated Carbon Observation System) Flask and Calibration Laboratory quality control work. In this program, three ~~high pressure cylinders (~~10L aluminum cylinders (Luxfer UK) are filled with dry air~~prepared~~ and maintained by the MPI-BGC and sent to measurement laboratories in a round robin loop. Two of the three cylinders had the same air mixture and showed small growth in their H_2 mole fractions over time. The third cylinder contains an "unknown" new mixture for each round robin loop.

Between 2016 and 2021, the MENI cylinders came to GML three times and were analyzed two to four times on the H9 instrument during each round robin stop ~~(see SI Figure 5)~~. Some results were rejected due to poor instrument performance or the use of an alternate calibration strategy than the one used to transfer the scale. For the blind and ambient ~~and blind~~ H_2 MENI cylinders the retained NOAA H_2 results agree well with the MPI_BGC measurements (< 1 ppb difference, SI Figure 5 a,b). For the low H_2 cylinder, the 2017/2018 NOAA measurements are biased low by about 2 ppb while the March 10, 2021 result is about 2 ppb higher (SI Figure 5c). The MENI program provides a~~n important~~ valuable on-going check for the MPI X2009 H_2 calibration scale transfer in GML.

2.3.3 Flask analysis systems ~~(H8, H11)~~ target air tanks

Figure 5a shows the calibration histories on H9 for target air tanks used in the flask analysis laboratory between 2009 and 2022. H_2 increased in all the target tanks, sometimes rapidly, requiring time dependent value assignments. ~~These time-dependent H_2 assignments are derived from the best linear or quadratic fit to the calibration results on H9. These assignments can be compared to the measurements on the flask analysis systems to evaluate the quality of the scale transfer~~ for the flask analysis system~~. It should be noted that the non-linear drift of some of these tanks may not be well modeled by a simple quadratic function, leading to higher uncertainty in the value assignments. This is especially true for tanks with limited calibration histories or gaps in their calibration histories.~~¶

Three H_2 target air tanks were in service between 2009 and 2019 and have been used to evaluate the GML calibration scale transfer to the MAGICC-1 and MAGICC-2 H_2 measurements (CC1824~~ (H)~~, CB08834 ~~(B)~~ and CC303036~~ (A)~~). These tanks, however, exhibited rapid and large drifts and were not measured on H9 on a regular basis making it more difficult to use them to evaluate potential biases on MAGICC-1 and MAGICC-2 over this time period.

The target air tanks ALMX067998 ~~(C)~~ and CB11143 ~~(C)~~ entered service in 2016 and 2019 respectively with more frequent measurements on the calibration system to better define their time dependent value assignments. A new set of six target air tanks were prepared at the Niwot Ridge facility in late 2019 for the MAGICC-3 system. They have been analyzed on MAGICC-3 multiple times a year but only one of them has a H_2 mole fraction that remained below 700 ppb: CB10292 ~~(B)~~.

With the caveats that the non-linear drift in aluminum cylinders may not be well modeled by a simple quadratic polynomial and that many of the early target tanks were under calibrated, the best polynomial fit to the calibration records for all target air tanks give residuals smaller than 1.2 ppb (Figure 5b). Details for the target tanks, including the best fit coefficients and the standard deviation of residuals to the fits are in SI Table 5~~S2~~. ~~The uncertainty on the assignments is larger during extended time periods with no calibration results especially for the 3 earlier target air tanks with a limited calibration history (CC1824 (H)) or with calibration histories showing evidence of a change in the drift rate (CB08834 (B) and CC303036 (A), see Figure 5).¶~~

In Figure 6, we show the differences between the target tank~~air~~ analysis results on H8 and H11 and their time-dependent H_2 assignments (based on the best fit to their calibration histories on H9 discussed above). The differences are all within 4 ppb, however there are ~~clearly~~ times when there are persistent biases between the flask analysis system(s) and the calibration system. Uncertainties on the value assignment of the target air tanks, the value assignments and stability of the standards used to calibrate the flask analysis systems as well as the noise in the H8 and H11 measurements all contribute to the observed differences. Similar offsets on both flask analysis systems (for example CC1824 prior to 2012) may point to the main uncertainty contribution being from the value assignment of the target air tank. Different patterns in the offsets between the two flask analysis systems (for example offsets of different signs for CC303036 ~~(A)~~ and CB08834 ~~(B)~~ on H8 and H11 in 2011-2013) suggest the offsets are due to value assignments of the flask analysis system standards. Again, this is often due to limited calibration histories not being able to fully map the non-linear drift in the standards. It also indicates there are times with systematic differences (mostly < 2ppb) between the MAGGIC-1/H11 and MAGICC-2/H8 measurements in the flask records.

The full transition to the new MAGICC-3 system for flask analyses in August 2019 is indicated by the vertical bar in Figure 6. As discussed earlier, one improvement in this new system is that H_2 measurements are now calibrated using a multi-point calibration curve from a suite of standards. This makes the measurement results less sensitive to drift or value assignment error in any individual standard since we are fitting multiple standards. ~~These standards are used once a month and thus have much longer lifetimes and longer calibration histories.~~ We also now appreciate the complex H_2 growth patterns that can occur in aluminum cylinders so have undertaken regular calibrations to ensure drift is tracked closely. These changes seem to have reduced the bias observed between the flask analysis system and the calibration system, which gives confidence that future measurements will be higher quality.

To help us monitor the H_2 calibration scale propagation performance going forward, a new target air tank in an Essex stainless steel cylinder, SX-1009237, was filled in late 2022 to augment the current target tanks. This target air tank should be stable for H_2 and will be used for periodic comparison between measurement systems. Analysis results on H9 and H11 in December 2022 are 526.75 and 527.15 ppb, respectively, consistent with the residuals for other target air tanks at that time.

3 NOAA flask air H_2 measurements

Close to 6000 flask air samples from the Cooperative Global Air Sampling Network are analyzed in GML every year. The network sites are chosen carefully to be representative of large scale air masses and to be able to rely on local support for sampling and shipping logistics. The reprocessing and release of the 2009-2021 H_2 global network flask air measurements on the MPI X2009 scale was made possible because of continued efforts to conduct and improve the H_2 measurements, to store all the necessary data, and to develop and update the tools for reliable and traceable reprocessing, comparison, and archiving.

3.1 Recapitulation of the GML flask air H_2 analysis system configurations since 2009

The MAGICC-2 H8 and MAGICC-1 H11 instruments started routine flask air H_2 analyses on November 5, 2009 and February 9, 2010 respectively. The flask air analysis results have been reprocessed using the tertiary standards or working standards time-dependent H_2 assignments on the MPI X2009 scale. As mentioned earlier, those flask air measurements on H8 and H11 until July 2019 relied on calibration with a single tertiary standard also used as reference to normalize the air sample chromatogram H_2 peak height.

After ABeginning in August 2019, the MAGICC-3 response was determined using multiple standards. multi-standard response the MAGICC-3 system uses a multi-standard instrument response calibration. For H_2, the instrument response curve is derived from eight working standards "known" assignments and their normalized H_2 peak heights, with a reference air that is not a standard. H8 was the H_2 instrument on MAGICC-3 until September 11, 2020 when it was replaced by H11 which has better precision. The linear fit coefficients for the MAGICC-3 H8 and H11 response curves are stored and used to calculate the H_2 dry air mole fraction in unknown air samples.

3.12 Data quality assurance and quality control

GML flask air H_2 measurements data quality is evaluated using results from the daily analysis of test air flask pairs and from the agreement between South Pole Observatory (SPO) flasks pairs.

In this section, we first describe the flask sample collection protocol and introduce the data quality control tags used to document sample and measurement data quality issues. GML flask air H_2 measurements data quality is evaluated using results from the daily analysis of test air flask pairs and from the agreement between South Pole Observatory (SPO) flask pairs. Then we assess the GML H_2 measurement short-term noise (repeatability) with statistics from test air flasks and SPOSouth Pole Observatory flask pair differences. Finally, we present a preliminary estimation for the uncertainty of flask air H_2 measurements over 2009-2021, that includes empirical uncertainty estimates for the standards' assignments and the short-term noise of the instruments.

3.12.1 Flask air sample collection overview and data quality tagging

Partners in the NOAA Cooperative Global Air Sampling Network collect whole outside air samples in glass flasks in pairs, upwind from any local sources of pollution, people and animals and away from structures or terrain that would affect the wind flow. Two 2.5L glass flasks with two glass stopcocks with Teflon o-rings are connected in series in a portable sampling unit (PSU) made of a rugged case, a battery, a pump, an intake line, and a mechanism to control the pressure of the air samples. Most sampling units include a dryer and are semi-automated, with the exception of those used at relatively dry high latitude locations and a few other locations where a more rugged, manually operated sampling unit is required. At most sites, the operator will carry the equipment outdoors to conduct the sampling. At a few sites, the PSU is indoors and connected to a fixed inlet line drawing air from the outside.

Before flasks are shipped to sampling sites,~~ment~~; the glass flasks are filled with synthetic air in the GML flask logistics laboratory. During the sample collection on site, the flasks are first flushed for several minutes and then filled to a pressure of 4 to 5 psi above ambient pressure in about 1 minute (See video: https://gml.noaa.gov/education/intheair.html).

Air sample collection and/or measurement issues that are documented or detected and known to affect a sample quality or an analyte measurement result are recorded with data quality control tags in our internal database. For each flask air measurement, internal data quality control tags are translated into a simpler 3 column flag indicating if the measurement is retained or rejected for external data users. The GML flask air samples and measurements can also have informational tags and comments, for example if another measurement laboratory analyzed an air sample before it came to GML for analysis (see same air ~~flask~~ measurement comparisons in section 3.3).

The global network flasks are filled to target pressure of 17-20 psia, but the final fill pressure can vary by 3-4~~a few~~ psi, with some of the higher altitude sites having final pressures on the lower range typically. If an air sample pressure is too low for the H_2 GC instrument on the MAGICC system, the H_2 measurement result is tagged as “rejected” for low sample pressure. If H_2 measurements in paired flasks have a 5 ppb or larger difference, the results for the pair are tagged as rejected. If only one member of the pair had an obvious issue (leak, low flask air pressure), only the H_2 measurement for that member is tagged as rejected. Some issues are detected by the MAGICC performance control system and are tagged automatically. Other issues are tagged manually by scientists as part of regular data quality control checks. Scientists also verify the validity of the automatic tags. Members of the team routinely evaluate if follow-up actions are needed to fix a sample collection or measurement~~n~~ issue or reduce the chance of rejecting future sample results for the same issue.

Some sites can experience brief high-pollution episodes with the H_2 mole fractions~~measurements~~ in both members of a pair meeting the pair agreement criteria but also being outliers, i.e. outside of the expected long-term variability at the site [Novelli et al., 1999]. Gross H_2 outliers are typically “tagged” manually. A statistical filter is applied before each annual data release [Dlugokencky et al., 1994]. For each site, ~~we applied~~ a smoothing curve fit calculation ~~to~~ determines the time series mean behavior broken down in a long-term trend, a seasonal cycle, and shorter-term (hours to weeks) variations [Thoning et al., 1989; Tans et al., 1989a]. The code is available and a link is provided further down. ~~Measurements that show large residuals from the fit are not representative of the typical background air composition at the site and are tagged as outliers [Novelli et al., 1999]. Gross H_2 outliers are typically “tagged” manually. We also apply a A statistical filter is applied before each annual data release [Dlugokencky et al., 1994]., which~~ The filter works iteratively to find and tag outlier H_2 measurements when their residuals to the smooth curve fit is larger than 3 to 4 times the time series residuals' standard deviation.

3.11~~2~~.2 Test air flask analysis results

Besides the regular analysis of target cylinders, the MAGICC flask analysis system is also ~~routinely~~ tested daily using flasks filled with "test air" (flasks with site code "TST"). ~~TST flasks are filled in one batch with air from one of~~ We have four rotating high pressure aluminum cylinders for test air (AL47-104, AL47-108, AL47-113, AL47-145), ~~themselves~~ filled at the Niwot Ridge standard preparation site. SI Figure 6 shows their calibration histories on H9 for different fills ~~for these four test air cylinders~~. H_2 is not stable in the "test air" cylinders and for some tank-fills, H_2 increased rapidly and grew beyond our calibration range upper limit of 700 ppb.

Every 2 to 3 weeks~~, the GML flask preparation and logistics laboratory manager fills~~ an even number of TST flasks (14-24) are filled from the same test air cylinder. On typical analysis days, the MAGICC flask air measurement sequence will start with the analysis of air from two TST flasks with the same fill date.

Global network flask air samples are analyzed at NOAA GML only during the daytime to ensure the system operator is overseeing the full analysis cycle and minimizing the time a flask valve is open for the analysis. This is meant to minimize the risk of losing or contaminating the air samples as many of them are subsequently sent to the University of Colorado Boulder Stable Isotopes Laboratory for CO_2 and CH_4 isotope analyses.

Results from the TST flask pairs with the same fill date and analyzed on successive days give an indication of the short-term repeatability of the measurements. Here, the deviations from the mean H_2 in TST flasks with the same fill date are evaluated. For fill dates with a mean H_2 mole fraction less than 700 ppb, we calculate the differences between individual TST flask H_2 and the fill date mean. The standard deviation of the TST flasks H_2 differences from their fill date mean is 1.39 ppb on MAGICC-2/H8 (N=872), 0.73 ppb on MAGICC-1/H11 (N=3583), 1.55 ppb on MAGICC-3/H8 (N=504) and 0.68 ppb on MAGICC-3/H11 (N=1085), reflecting the higher measurement noise on H8.

Another diagnostic is the comparison of the TST flasks H_2 results and their test air cylinders' time-dependent assignments for the dates the TST flasks were filled based on the best fit of the H9 test air tank calibration results. This analysis is limited to the test air ~~cylinders and fill code(s)~~ with less than 700 ppb H_2 and with tank calibration results on H9 that reasonably capture the increase in H_2: AL47-108 (F), AL47-113 (D,E,G), AL47-145 (F,G), AL47-104 (I). In SI Figure 7 (a-c), we show the H_2 differences between the TST flask results and their test air cylinder assignments. The differences reflect noise in the flask air measurements and uncertainties (and potentially small biases) in the test air tank-fill assigned H_2.

Between 2010 and 2021, ~~T~~the three fills of test air cylinder AL47-113 are in the ambient range and have the most stable H_2 mole fractions. The tank-fill assigned H_2 linear drift rate is 1 ppb/yr in fill D, null in fill E and 0.4 ppb/yr in fill G. Table 3~~5~~ shows the mean and standard deviation of the differences in H_2 between TST flasks and the assigned H_2 in a stable or slowly drifting test air tank-fill. The biases for these subsets of TST air data are less than 1 ppb and the standard deviation is equal to or less than 1.5 ppb and is smaller for the most recent MAGICC-3/H11 configuration which has a smaller number of data points.

3.112.3 South Pole Observatory: H_2 differences in flask pairs

NOAA GML operates four staffed atmospheric baseline observatories (https://gml.noaa.gov/obop/). The South Pole Observatory (SPO) in Antarctica and the Mauna Loa (MLO, Hawaii) observatories were built in connection with the 1957-1958 International Geophysical Year, a global effort bringing together 67 nations to study the Earth and in connection with the first launches of artificial satellites in Earth's orbit by the USA and the Soviet Union. The South Pole Observatory in Antarctica was established with support from the US National Science Foundation and NOAA. The other two observatories near Utqiaġvik, formerly Barrow, (BRW) and Samoa (SMO) were established in 1973 and 1974 respectively. H_2 time series for the observatories are shown in section 4. Two flask pairs are typically collected weekly and close in time at the four NOAA atmospheric baseline observatories using two collection methods. In method 'S', flasks are filled inside a building by tapping the air continuously pumped for analysis on an in-situ GHG measurement system. Method, 'P' (or 'G') involves using a portable sampling unit with an inlet mast and pump set up outside the building, similarly to other global network sites.

The South Pole Observatory (site code SPO, sampling location: 89.98°S, 24.80°W, 2815 meters above sea level (masl)) gives scientists access to some of the "cleanest" air on Earth due to its remote location, and thus provides an opportunity to use SPO flask data as a quality assurance tool.. On site, GML and partners operate in-situ measurements to monitor the atmosphere composition and properties, and whole air samples have been collected for trace gas analyses in the GML laboratories in Boulder since 1975.

All four NOAA atmospheric baseline observatories have an upwind clean air sector with no local sources of pollution (https://gml.noaa.gov/obop/). Every week, scientists on location collect discrete air samples when the near surface wind comes from the clean air sector. Two flask pairs are typically collected weekly and close in time at the four NOAA atmospheric baseline observatories using two collection methods. In method 'S', flasks are filled inside a building by tapping the air continuously pumped for analysis on an in-situ GHG measurement system. Method, 'P' (or 'G') involves using a portable sampling unit with an inlet mast and pump set up outside the building , similarly to other global network sites. The scientist doing the air sampling is involved with both sampling techniques. Weekly samples with both methods are typically conducted within minutes of each other. Both flask sampling methods give reliable results for H_2 at the South Pole Observatory.

Staff rotation and flask shipping to and from the South Pole Observatory happen during a limited time window during the Austral summer. While awaiting shipment, SPO flask air samples are stored in crates in a heated storage building. Every year, one large SPO flask shipment arrives in Boulder in December/January and another smaller shipment arrives in February/March. A year's worth of flasks is prepared and shipped to SPO during that same time window. Despite the longer storage for SPO flasks before analysis, we have not detected biases in H_2 measurements of those samples when compared with other high southern latitudes times series. SPO flask air H_2 measurements show close to a 20 ppb seasonal cycle and a ~15 ppb increase in the annual mean levels between 2010 and 2021 (Figure 7).

There is very little short-term variability in the surface air over Antarctica for long-lived GHGs, CO and H_2. The differences in the H_2 mole fractions in SPO paired samples therefore mostly reflect the short-term noise in the measurements. In SI Table 6 we report statistics for H_2 differences for the two flask sampling methods and the four measurement system configurations between 2009 and 2021 with H8 and H11. As observed for the TST flasks, measurements on H11 are less noisy than on H8, especially on the MAGICC-3 system. The average of the absolute differences for H_2 in SPO flask paired samples is less than 2 ppb ($\sigma \leq 1.3$ ppb) and methods S and P H_2 pair averages at SPO agree within 1 ppb on average ($\sigma \leq 1.7$ ppb). ¶

3.1~~2~~.4 Flask air H_2 uncertainty estimates

We have derived preliminary empirical uncertainty estimates for flask air H_2 measurements that fall in the 200-700 ppb range. For measurements on MAGICC-1 and MAGICC-2, the total uncertainty estimate comes from the combination of two uncertainties added in quadrature: 1) the uncertainty on the H_2 tertiary standard time-dependent assignment (SI Table 2) and 2) the instrument estimated repeatability (Table 4~~8~~). If an offline assignment correction is applied to take into account changes in a standard drift rate toward the end of its use, the standard assignment uncertainty is increased. The H8 and H11 instrument repeatability estimates are listed in Table 4~~8~~. For now, we assume a 0.5 ppb uncertainty on the MAGICC-3 instrument response calibrated with multiple standards. On-going work will allow us to refine this last uncertainty component estimate at a later date. Typical 1-sigma uncertainties for GML flask air H_2 measurements are 1.2 to 1.9 ppb on MAGICC-1, 1.4 to 2.8 ppb on MAGICC-2, 1.6 ppb on MAGICC-3/H8 and 0.8 ppb on MAGICC-3/H11.

3.2~~3~~ Comparison with other GAW laboratories H_2 measurements

A small number of laboratories operate well-calibrated long-term measurements of important atmospheric trace gases. The WMO Global Atmospheric Watch (GAW) coordinates regular technical and scientific discussions with experts from these laboratories. Another important outcome of the WMO/GAW collaborations consists of routine comparisons to assess the data compatibility for measurements ~~coming~~ from different laboratories and programs [Francey et al., 1999; Masarie et al., 2001; Jordan and Steinberg, 2011; Worthy et al., 2023]. The WMO/GAW network compatibility goals for measurements of H_2 in well mixed background air is 2 ppb (see Table 1 in [WMO/GAW, 2020]). This means that for H_2, measurement records should not have persistent biases less than 2 ppb to be used in combination with other qualifying measurements in global budget, trend and large scale gradient analyses.

GML participates in several WMO GAW measurement comparison efforts. Same-flask air measurement comparisons consist of one member of a NOAA flask pair collected at a site being analyzed by a partner laboratory before being analyzed by GML. Co-located flask air measurement comparisons involve 2 or more measurement programs having samples collected at the same location and close in time. Historically, these and other "intercomparison" projects have been abbreviated ICPs, which we use in the text below. Here the GML flask air H_2 measurements data compatibility is assessed with results from on-going ICPs.

GML conducts same-flask air measurement comparisons at the Cape Grim Observatory (CGO, 40.68º S, 144.69º W,164 masl) with CSIRO, Australia and at the Ochsenkopf mountain top tower (OXK, 50.03º N, 11.81º E, 1085 masl) with MPI-~~/~~BGC, Germany. Sampling at OXK was temporarily suspended between June 2019 and April 2021. The Alert/Dr Neil Trivett Observatory (ALT, 82.45º N -62.51º W, 190 masl) has facilitated the largest multi-laboratory flask air comparison experiment in the WMO GAW program [Worthy et al., 2023]. NOAA has colocated flask air samples from ALT with CSIRO and the MPI-~~/~~BGC. The CSIRO and MPI-~~/~~BGC H_2 measurements are also traceable to the MPI X2009 calibration scale.

In Table 5~~7~~, we summarize the annual mean of the differences for H_2 measurements from different laboratory and flask combinations (same flask, same flask pair or collocated flasks) for CGO, OXK and ALT between 2010 and 2021. ~~Columns 2 and 3 show the annual means of the NOAA H_2 differences between the ICP flask and its pair mate at CGO and OXK.~~ All measurements included in the comparisons are retained, meaning they have passed quality control checks.

Columns 2 and 3 show the annual means of the NOAA H_2 differences between the ICP flask and its pair mate at CGO and OXK. For CGO flask air samples collected before 2019, we find that the NOAA analysis for the NOAA ICP flask first measured at CSIRO often shows higher H_2 than in the non-ICP flask air sample. We suspect several of these ICP flasks had a small but detectable contamination for H_2. We have applied a rejection tag to NOAA analysis results for CGO ICP flasks with an H_2 mole fraction 2 ppb or more above H_2 in the non-ICP pair mate. This affected 165 ICP samples between 2009 and 2018 or 37% of all CGO ICP flasks collected between August 2009 and the end of 2021. ¶

¶

For OXK, the NOAA analysis result for the ICP flask first measured at MPI-~~/~~BGC often shows slightly higher H_2 than in the non-ICP flask (Table 5~~7~~, 3rd column), and the annual mean bias is less than 1 ppb for all years.

The last 4 columns in Table 5~~7~~ show interlaboratory H_2 measurement comparisons for CGO, OXK and ALT flask air samples. The annual mean differences are consistently less than 1.6 ppb for CGO ~~(CSIRO ICP flask and NOAA non ICP flask)~~ and less than 2 ppb for OXK for 9 out of 11 years ~~(MPI/BGC ICP flask and NOAA ICP flask)~~ (Figure 8). For colocated air samples at ALT ~~(NOAA vs CSIRO and NOAA vs MPI/BGC)~~ we compare the mean of flask results for each laboratory and limit the comparison for samples collected within 60 minutes of each other. The ALT annual mean differences vary from year to year, and are less than +/- 2 ppb for 8 years out of 12 for the NOAA vs CSIRO comparison and for 7 years out of 10 for the NOAA vs MPI-~~/~~BGC comparison. These on-going ICPs are monitored regularly to continually assess the NOAA H_2 data compatibility with data from GAW partners.

4. NOAA ~~H_2~~ atmospheric H_2 time series

Previous measurement studies have described ~~key features of~~ the H_2 global distribution for different time periods [Khalil and Rasmussen, 1990; Novelli et al., 1999; Langenfelds et al., 2002; Price et al., 2007; Yver et al., 2011]. Some of the spatiotemporal features in the more recent NOAA H_2 measurement records ~~measurements at background sites~~ are described in this section.

4.1 H_2 at the NOAA Cooperative Global Air Sampling Network Sites

There are 51 sites considered active or recently terminated in the Cooperative Global Air Sampling Network (see map in SI Figure 8 and site information in SI Table 7). The H_2 measurement times series for these sites are shown in SI Figure 9. Note that a few sites that have been discontinued are not shown in this figure. A curve fit is run for each site time series based on Thoning et al. [1989]. First the code optimizes parameters for a function made of a four-term harmonic and a cubic polynomial. The resulting residuals (measurements minus function) are then smoothed with a low-pass filter with a 667-day cutoff and are added to the polynomial part of the function to produce the “trend curve” (shown as the dark blue line in SI Figure 9). The residuals are also smoothed with a low-pass filter with a 80 day cutoff and are added to the function to produce a “smooth curve” at each site.

The data quality control work on our long-term measurement time series includes a data selection step with a statistical filter (see section 3.1.1). Samples with H_2 beyond 3.5 (4 for Ascension Island, ASC) standard deviations of the time series smoothed curve at each site are flagged as not representative of background air conditions and are shown as crosses in SI Figure 9.

The annual mean, maximum and minimum H_2 values of the smooth curve for the 51 sites are plotted in Figure 9 (in order of decreasing latitude along the x-axis) for years with retained measurements up to 2021. Sampling at the TPI site, on Taiping Island, Taiwan, started in May 2019, which explains the 2 (full sampling year) data points for the site. Sampling at a few network sites was impacted by the COVID-19 pandemic resulting in data gaps or delayed return shipping of samples. We recommend data users become familiar with individual sampling site measurement records to best aggregate and interpret signals.

The interhemispheric gradient of H_2, with higher levels in the SH, is apparent in the annual means distribution across sites (Figure 9, green circles). The majority of sites in the SH (BKT to SPO on the right side of Figure 9) show smaller seasonal cycle amplitudes (<23 ppb) than NH sites; however, several sites have interannual variations in their H_2 seasonal cycle amplitudes (SI Figure 9). Sites with the lowest H_2 seasonal minima (Figure 9, blue x symbols) likely are the most influenced by soil uptake. A few sites (for ex. TAP (Taiwan), AMY (Republic of Korea), LLN (Taiwan), CPT (South Africa)) show higher smooth curve annual maxima (Figure 9, red crosses), likely reflecting upwind local or regional emissions.

4.2 H_2 at NOAA Baseline Atmospheric Observatories

NOAA GML operates four staffed atmospheric baseline observatories (https://gml.noaa.gov/obop/). The South Pole Observatory in Antarctica and the Mauna Loa (MLO, Hawaii) observatories were built in connection with the 1957-1958 International Geophysical Year, a global effort bringing together 67 nations to study the Earth and in connection with the first launches of artificial satellites in Earth’s orbit by the USA and the former Soviet Union. The South Pole Observatory in Antarctica was established with support from the US National Science Foundation and NOAA. The other two observatories near Utqiaġvik, formerly Barrow, (BRW) and Samoa (SMO) were established in 1973 and 1974 respectively.

All four NOAA atmospheric baseline observatories have an upwind clean air sector with no local sources of pollution. Every week, scientists on location collect discrete air samples preferentially when the near surface wind comes from the clean air sector. Figure 10~~9~~ shows the reprocessed H_2 time series for the ~~four NOAA Baseline Atmospheric~~ Observatories between 2009 and 2021. Valid “S” and “P” method flask air H_2 measurements are retained for the South Pole Observatory only. The “S” method flasks show contaminated H_2 at Samoa and show seasonal~~some~~ contamination ~~or more variable H_2~~ at Utqiaġvik (Barrow) until August 2021 when sampling started at a new tower with new sampling lines. The Mauna Loa H_2 in “S” method flasks will be further evaluated and may be retained in future releases.

The Samoa and South Pole H_2 smooth curves ~~flask air measurements~~ show similar maximum levels between 550 and 570 ppb and slightly higher minima at Samoa compared to the South Pole. The seasonal maximum~~a~~ occurs about 3 months earlier at Samoa than at the South Pole. The interannual variability is similar at both sites and is dominated by step increases on three occasions: in 2012/2013, 2016 and 2020.

The Mauna Loa H_2 time series shows more short-term variability than for Samoa and South Pole. ~~reflecting the variable latitudes covered by an air mass before it is sampled at the high-altitude observatory and the strong spatial gradients for H_2 in the NH.~~ The mean seasonal cycle amplitude of the~~at~~ Mauna Loa H_2 smooth curve is about 40 ppb with maximum levels in April-May and minimum levels in December-January. The ~~observed~~ seasonal maximum~~a~~ ranges from 550 to 580 ppb and the ~~observed~~ seasonal minimum~~a~~ ranges from 505 to 520 ppb. The ~~NOAA~~ measurements indicate that annual mean H_2 levels at Mauna Loa after 2016~~8~~ were higher than in previous years.

Of the four observatories, the Barrow H_2 time series shows the lowest levels and the strongest seasonal cycle, about 60 ppb on average. The smooth curve ~~observed~~ seasonal maximum ranges from 520 to 540 ppb in April-May and the ~~observed~~ seasonal minimum in September-November ranges from 450 to 490 ppb.

Despite having larger emissions in the NH, the H_2 interhemispheric gradient shows lower levels in the extratropical NH. This is related to the larger land masses in the NH and the soil sink being the dominant removal process for H_2. Warwick et al. [2022] report model-based estimates for the H_2 lifetime of 8.3 years for the OH sink (from the authors base model configuration) and of 2.5 years for the soil uptake (average of existing literature studies). In their flux inversion, Yver et al. [2011] estimated that the NH high latitudes and the tropics represent 40% and 55% of the global soil sink respectively. The soil sink and OH sink in extratropical northern latitudes both peak in summertime [Price et al., 2007] leading to the observed stronger H_2 minima.

~~Given the larger variability and stronger seasonality of H_2 in the NH extra tropics, i~~It is important to look at data from multiple sites to study and detect interannual and potentially long-term large-scale changes in atmospheric H_2 levels. In the next section, we ~~highlight a few features in the global network H_2 records and~~ present background air zonal mean H_2 time series based on samples collected at marine boundary layer sites.

~~4.2 H_2 at the NOAA Global Cooperative Air Sampling Network Sites¶~~

~~There are 51 sites considered active or recently terminated in the Global Cooperative Air Sampling~~

Network (see map in SI Figure 8). The H_2 measurement times series for these sites are shown in SI Figure 9. Note that a few sites that have been discontinued are not shown in this figure. A curve fit is run for each site time series based on Thoning et al. [1989]. First the code optimizes parameters for a function made of a four-term harmonic and a cubic polynomial. The resulting residuals (measurements minus function) are then smoothed with a low-pass filter with a 667-day cutoff and are added to the polynomial part of the function to produce the "trend curve" (shown as the dark blue line in site time series plots in SI Figure 9). The residuals are also smoothed with a low-pass filter with a 80 day cutoff and are added to the function to produce a "smooth curve" at each site. ¶

The data quality control work on our long-term measurement time series includes a data selection step [Dlugokencky et al., 1994]. Samples with H_2 beyond 3.5 (4 for ASC) standard deviations of the time series smoothed curve at each site are flagged as not representative of background air conditions and are shown as crosses in SI Figure 9.¶

The annual mean, maximum and minimum H_2 values of the smooth curve for the 51 sites are plotted in Figure 10 (in order of decreasing latitude along the x-axis) for years with retained measurements up to 2021. Sampling at the TPI site, on Taiping Island, Taiwan, started in May 2019, which explains the 2 (full sampling year) data points for the site. Sampling at a few network sites was impacted by the covid-19 pandemic resulting in data gaps or delayed return shipping of samples. We recommend data users become familiar with individual sampling site measurement records to best aggregate and interpret signals.¶

The interhemispheric gradient of H_2, with higher levels in the SH, is apparent in the annual means distribution across sites in Figure 10 (green circles). The majority of sites in the SH (BKT to SPO on the right side of Figure 10) show smaller seasonal cycle amplitudes (<23 ppb) than NH sites; however, several sites have interannual variations in their H_2 seasonal cycle amplitudes (SI Figure 9). Sites with the lowest H_2 seasonal minima (Figure 10, blue x symbols) likely are the most influenced by soil uptake. A few sites (for ex. TAP, AMY, LLN, CPT) show higher smooth curve annual maxima (Figure 10, red crosses), likely reflecting upwind local or regional emissions. ¶

Two sites, KUM and WIS, had a change of sampling location that resulted in visibly different H_2 mean levels and seasonal cycle amplitudes. In mid 2018, the KUM site was moved 30 km NNW along the Hawaii island SE coastline when access to a lava field bordering the ocean was lost in the eruption of the Kīlauea volcano. The KUM sampling location change resulted in higher mean H_2 levels and a smaller seasonal cycle. The WIS site moved 100 km SSE in Israel in early 2015. There are more instances of depleted H_2 (in December-March) since the move, potentially reflecting a stronger influence of soil uptake in air masses sampled at the newer location.

4.3 H_2 marine boundary layer global and zonal means

To extract large scale signals from the global air sampling network, we use the NOAA GML marine boundary layer (MBL) zonal data product [Tans et al., 1989b; Dlugokencky et al., 1994]. Time series from remote MBL sites are smoothed and interpolated to produce a latitude versus time surface of the H_2 mean MBL mole fraction (Figure 11). For H_2, the number of sites included in the zonal mean calculations ranges from 29-42 sites until July 2017 when sampling from the Pacific Ocean shipboard (POC) was stopped, after which 24-27 sites were included in the calculation. Because the Cooperative Global Air

Sampling Network is sparse in the tropics and in the SH mid latitudes, the MBL product likely does not equally detect and reflect interannual variability in fluxes in these under-sampled regions, for example biomass burning emissions in Africa and South America.

To further isolate changes in background H_2 at different latitudes, we first calculate MBL global ~~(~~and zonal ~~band)~~ means (shown in SI Figure 10) and then derive anomalies by removing the 2010-2021 average year from the global and~~(or~~ zonal ~~band~~ mean~~)~~ time series. Figure 12 shows the MBL anomaly for H_2 (black lines) and CO (dashed blue lines) for the global mean and 5 zonal band means (NH and SH Polar (53-90º), NH and SH Temperate (17.5-53º) and Tropics (17.5ºS to 17.5ºN). The NOAA GML CO measurements are for the same air samples as the H_2 measurements [Pétron et al., 2023b]. Here, we derive the global and zonal means for CO using the 2009-2022 MBL CO measurements and the anomalies are based on the 2010-2021 smooth curve zonal mean results to be consistent with the H_2 data analysis.

CO is emitted during incomplete combustion and is a useful marker of biomass burning emissions. CO has a shorter atmospheric lifetime than H_2 which results in shorter-lived CO anomalies from pulse emissions. The data reduction for the anomaly analysis is slightly different from Langenfelds et al. [2002] investigation of CO_2, CH_4, H_2, and CO interannual variability in the CSIRO network 1992-1999 time records. The CSIRO authors employed the same [Thoning et al., 1989] data smoothing technique as we do but used the derivative of the trend curve to analyze correlations in interannual growth rate variations between species. The anomaly approach chosen here allows to retain the timing of abrupt changes in the measurement records.

Over 2010-2021, background air H_2 has increased at all latitudes (Figure 12). The global mean MBL H_2 shows a non-uniform increase over this time with a noticeable 10 ppb step increase in 2016. The global mean MBL H_2 was 20.2 ±0.2 ppb higher in 2021 compared to 2010 (Figure 12a).

The meridional gradient and zonal band mean plots (Figures 11 and ~~Figure~~ 12~~b-f~~) highlight the evolution of background air H_2 at different latitudes. ~~By construction, the smooth curve anomalies are not directly proportional to the biomass burning emissions that likely~~ may have ~~caused them. Rather the a~~Anomalies in the smooth curves are useful to point to time periods when several successive air samples at a site show similar deviations from the average seasonal cycle and multi-year trend.

The 2016 H_2 step increase is detected in the Tropics and SH. In the Tropics it coincides with a strong positive CO anomaly that started in November 2015, reached a peak amplitude of 15 ppb mid-January 2016 and ended in May 2016. The 2015/2016 H_2 anomaly is first detected at Bukit Kototabang, Indonesia (BKT) and later at Ascension Island (ASC), Cape Grim (CGO) and Crozet Island (CRZ) (SI Figure 11). Some BKT air samples impacted by biomass burning emissions show enhancements of 100s ppb in CO and H_2. ~~The BKT CO and H_2 data also show enhancements likely related to biomass burning in 2015.~~ The 2015 fire season in Indonesia was among the most intense on record as shown by remote sensing products of fire counts, CO and aerosols. Field et al. [2016] found that burning activities to clear peatland for farming likely contributed to larger emissions than expected from dry conditions alone in 2015.

There is another step increase in the Polar SH zonal band in early 2020, also coinciding with a pulse anomaly in CO (Figure 12f) likely related to large wildfires in Australia in late 2019-early 2020. The Cape Grim (CGO) and Crozet Island (CRZ) smoothed curves show a large jump between the late 2019 minimum and early 2020 maximum when the CGO CO measurement seasonal minimum is also 10-12 ppb higher than in other years (SI Figure 11). van der Welde et al. [2021] estimate that the 2019-2020 fires in Australia emitted 80% more CO_2 than “normal” Australian annual fire and fossil fuel emissions combined.

In the NH extratropics bands, positive anomalies in H_2 in 2021 coincide with CO pulse anomalies. For the Polar (Temperate) NH zonal band, the CO anomaly lasts from mid-July (June) to December 2021 with a peak in September and an anomaly maximum amplitude of 37 ppb (19 ppb). Record high emissions of CO_2 and CO from boreal forest fires in Eurasia and North America in 2021 have been reported by Zheng et al. [2023].

Previously, Simmonds et al. [2005] and Grant et al. [2010] have reported on the observed variability in the Mace Head continuous H_2 measurement record and linked interannual variability in the baseline annual mean H_2 to larger fire emission events. More recently, Derwent et al. [2023] shared an updated analysis of the February 1994-September 2022 Mace Head in-situ H_2 measurements. The in situ record shows higher monthly mean baseline H_2 levels in recent years and the authors report an increase in monthly mean anomalies after December 2015 (slope of 2.4 +/- 0.5 ppb/yr). They postulate that a “missing” source of increasing intensity after 2010 may be behind the observed sustained increased H_2, which is markedly different from the 1998-1999 anomalies attributed to biomass burning. Derwent et al. [2023] explore potential candidates for the missing sources. However, in the absence of strong and quantitative direct evidence at this time, additional studies are needed to interpret the observed H_2 variability.

5. Conclusions

In this paper, we have described how NOAA GML has adopted the MPI X2009 H_2 calibration scale. The work was confined to measurements on GC-HePDD instruments. The GML H_2 primary standards in electropolished stainless steel cylinders have been calibrated once by the MPI-BGC CCL in Fall 2020. We have used the CCL assignments to propagate the scale to secondary and tertiary standards. H_2 increases in most air standards stored in aluminum cylinders. A curve fit wais applied to each standard calibration history to determine a time-dependent H_2 assignment on MPI X2009. The secondary and tertiary and working standards H_2 assignments were then used to reprocess results for NOAA flask air H_2 measurements on MPI X2009. These NOAA Cooperative Global Air Sampling Network flask reprocessed H_2 measurements for 2009-2021 are now publicly available [Pétron et al., 2023a]. For the period 2010-2021, same air measurements with GAW partner laboratories have annual mean differences less than 2 ppb for the Cape Grim comparison with CSIRO and less than 3 ppb for the Ochsenkopf comparison with MPI BGC. Over 2010-2021, background air H_2 has increased at all latitudes. However, site time series and marine boundary layer H_2 zonal means show significant interannual variability. We find that some of strongest H_2 zonal mean anomalies coincide with CO anomalies and therefore were likely partly driven by large biomass burning events in Indonesia (2015), Australia (2019/2020), and boreal latitudes (2012 and 2021) [Field et al., 2016; Petetin et al., 2018; Zheng et al., 2023]. A full analysis of the NOAA Cooperative Global Air Sampling Network H_2 measurement records is beyond the scope of this paper. This dataset complements WMO/GAW partner laboratories H_2 measurements and it will be updated and extended routinely moving forward.

Data and Code Availability

The NOAA global network flask air H_2 and CO time series are available at https://doi.org/10.15138/WP0W-EZ08.

We kindly request that users of the NOAA H_2 dataset cite:

Pétron, G., Crotwell, A., Crotwell, M., Kitzis, D., Madronich, M., Mefford, T., Moglia, E., Mund, J., Neff, D., Thoning, K., & Wolter, S. (2023). Atmospheric Hydrogen Dry Air Mole Fractions from the NOAA GML Carbon Cycle Cooperative Global Air Sampling Network, 2009-2021 [Data set]. NOAA GML CCGG Division. Version: 2023-05-25, https://doi.org/10.15138/WP0W-EZ08

The python class used to filter and smooth time series data is available and explained at: https://gml.noaa.gov/aftp/user/thoning/ccgcrv/ccgfilt.pdf and the method can be referenced as [Thoning et al., 1989].

Supplement

The supplement for this article is available in a separate file.

Author Contributions

GP and AC designed the scale revision work. GP, AC and JM implemented the scale revision. GP, AC, MC, MM, DN and JM contributed to the data quality control. GP and JP analyzed network site time series. AC designed, built and oversaw the H_2 calibration scale transfer and the flask air analysis system operations, working with Paul Novelli until he retired in 2017. TM and AC carried out tank calibrations. BH prepared the primary standards. DK was in charge of the whole air ~~secondary and tertiary~~ standards, reference, target and test air tanks preparation. MM and EM were responsible for the flask air analysis lab operations, working with Patricia Lang until her retirement in 2019. EM managed the flask logistics laboratory and flask metadata entries. DN with support from SW managed the NOAA Cooperative Global Air Sampling Network. DN managed sampling equipment for sites. JM manages the database and date releases.~~;~~ JM, KT and AC developed code and user interfaces for data processing, quality control and exploration. AJ calibrated the NOAA primary standards. AJ, PK and RL contributed data from their measurement programs. GP prepared the manuscript with contributions from AC and AJ and edits from BH, MC, RL, and JP.

Competing Interests

The authors declare that they have no conflict of interest.

Acknowledgements

We are grateful for our partners worldwide who collect and ship flask air samples to NOAA GML, Boulder, CO for analysis. We thank past and current NOAA GML and CU CIRES colleagues for their contributions to the network operations, measurements, data management and data quality control. Special thanks also go to Victoria Marin from the NOAA Climate Program Office and to Fabien Paulot from the NOAA Geophysical Fluid Dynamics Laboratory for their assistance and their leadership with the H_2 interagency project respectively. Gary Morris and Kathryn McKain from GML, Simon O'Doherty and an anonymous referee provided valuable comments on the manuscript.

~~Gary Morris, and Kathryn McKain, Simon O'Doherty and an anonymous referee provided valuable comments on the manuscript.~~

Financial support

This work~~research~~ was supported in part by NOAA C~~c~~ooperative A~~a~~greements NA17OAR4320101 and NA22OAR4320151 and~~. This material is based upon work supported~~ by the U.S. Department of Energy's Office of Energy Efficiency and Renewable Energy (EERE) under the Hydrogen and Fuel Cell Technologies Office (HFTO). The views expressed herein do not necessarily represent the views of NOAA, the U.S. Department of Energy or the United States Government.

References

Bertagni, M.B., Pacala, S.W., Paulot, F. et al. Risk of the hydrogen economy for atmospheric methane. Nat Commun 13, 7706, doi: 10.1038/s41467-022-35419-7, 2022.

Brito J., Wurm, F., Yáñez-Serrano, A. M., de Assunção, J. V., Godoy, J. M., and Artaxo, P., Vehicular Emission Ratios of VOCs in a Megacity Impacted by Extensive Ethanol Use: Results of Ambient Measurements in São Paulo, Brazil, Environmental Science & Technology, 49 (19), 11381-11387, doi: 10.1021/acs.est.5b03281, 2015.

Ciais P., Tans, P. P., Trolier, M., et al., A Large Northern Hemisphere Terrestrial CO_2 Sink Indicated by the $^{13}C/^{12}C$ Ratio of Atmospheric CO_2. Science 269,1098-1102, doi: 10.1126/science.269.5227.1098, 1995.

Conway, T. J., Tans, P. P., Waterman, L. S., Thoning, K. W., Kitzis, D. R., Masarie, K. A., and Zhang, N., Evidence for interannual variability of the carbon cycle from the National Oceanic and Atmospheric Administration/Climate Monitoring and Diagnostics Laboratory Global Air Sampling Network, J. Geophys. Res., 99(D11), 22831–22855, doi:10.1029/94JD01951, 1994.

Cooper O.R., Schultz M. G., Schröder S., et al.; Multi-decadal surface ozone trends at globally distributed remote locations. Elementa: Science of the Anthropocene; doi:10.1525/elementa.420, 2020.

de Kleijne, K., de Coninck H., van Zelm, R., Huijbregts M. A., and V. Hanssen S. V., The many greenhouse gas footprints of green hydrogen, Sustainable Energy Fuels, 6, 4383-4387, doi: 10.1039/D2SE00444E, 2022.

Derwent, R. G., Simmonds, P. G., O'Doherty, S., Manning, A. J., Spain, T. G., High-frequency, continuous hydrogen observations at Mace Head, Ireland from 1994 to 2022: Baselines, pollution events and 'missing' sources, Atmospheric Environment, Volume 312, doi: 10.1016/j.atmosenv.2023.120029, 2023.

Dlugokencky, E. J., Steele, L. P., Lang, P. M., and Masarie, K. A., The growth rate and distribution of atmospheric methane, *J. Geophys. Res.*, 99(D8), 17021– 17043, doi:10.1029/94JD01245, 1994.

Dlugokencky, E. J., Bruhwiler, L., White, J. W. C., et al., Observational constraints on recent increases in the atmospheric CH_4 burden, Geophys. Res. Lett., 36, L18803, doi:10.1029/2009GL039780, 2009.

Field, R. D., van der Werf, G. R., Fanin, T., et al., Indonesian fire activity and smoke pollution in 2015 show persistent nonlinear sensitivity to El Niño-induced drought. Proceedings of the National Academy of Sciences 113, 33(2016), 9204–9209, doi: 10.1073/pnas.1524888113, 2016.

Francey, R. J.; Steele, L. P. ;Langenfelds, R. L.; and B.C. Pak, High Precision Long-Term Monitoring of Radiatively Active and Related Trace Gases at Surface Sites and from Aircraft in the Southern Hemisphere Atmosphere, Journal of Atmospheric Sciences, pp. 279-285, https://doi.org/10.1175/1520-0469(1999)056%3C0279:HPLTMO%3E2.0.CO;2, 1999.

Francey, R. J.; Steele, L. P.; Spencer, D. A.; Langenfelds, R. L.; Law, R. M.; Krummel, P. B.; Fraser, P. J.; Etheridge, D. M.; Derek, N.; Coram, S. A.; Cooper, L. N.; Allison, C. E.; Porter, L.; Baly, S. The CSIRO (Australia) measurement of greenhouse gases in the global atmosphere. In: Report of the eleventh WMO/IAEA Meeting of Experts on Carbon Dioxide Concentration and Related Tracer Measurement Techniques; 2001; Tokyo, Japan. World Meteorological Organization; pp. 97-106. http://hdl.handle.net/102.100.100/194315, 2003. Last accessed December 29, 2023.

Friedlingstein, P., et al., Global Carbon Budget 2022, Earth Syst. Sci. Data, 14, 4811–4900, https://doi.org/10.5194/essd-14-4811-2022, 2022.

Grant, A., Witham, C. S., Simmonds, P. G., Manning, A. J., and O'Doherty, S.: A 15 year record of high-frequency, in situ measurements of hydrogen at Mace Head, Ireland, Atmos. Chem. Phys., 10, 1203–1214, doi: 10.5194/acp-10-1203-2010, 2010.

Heiskanen, J. et al., The Integrated Carbon Observation System in Europe. Bulletin of the American Meteorological Society 103 (3), pp. E855 - E872, doi: 10.1175/BAMS-D-19-0364.1, 2022.

Hydrogen Council and McKinsey & Company, Hydrogen Insights 2023, 23pp. Accessible at: https://hydrogencouncil.com/wp-content/uploads/2023/12/Hydrogen-Insights-Dec-2023-Update.pdf, 2023. Last accessed December 29, 2023.

International Energy Agency, Global Hydrogen Review 2022, IEA, Paris, https://www.iea.org/reports/global-hydrogen-review-2022, License: CC BY 4.0, 284pp, 2022. Last accessed December 29, 2023.

Jordan, A. and Steinberg, B.: Calibration of atmospheric hydrogen measurements, Atmos. Meas. Tech., 4, 509–521, doi: 10.5194/amt-4-509-2011, 2011.

Khalil, M. A. K., and Rasmussen, R. A., Seasonal cycles of hydrogen and carbon monoxide in the polar regions: Opposite phase relationships, Ant. J. U. S. , 23(5), 177-178, 1989.

Khalil, M. A. K. and Rasmussen, R. A., Global increase of atmospheric molecular hydrogen. Nature 347, 743–745, doi: 10.1038/347743a0, 1990.

Kitzis, D., Preparation and Stability of Standard Reference Air Mixtures, 2017. https://gml.noaa.gov/ccl/airstandard.html. Last accessed May 17, 2023.

Komhyr, W. D., R. H. Gammon, T. B. Harris, L. S. Waterman, T. J. Conway, W. R. Taylor, and K. W. Thoning, Global atmospheric CO_2 distribution and variations from 1968–1982 NOAA/GMCC CO_2 flask sample data, J. Geophys. Res., 90(D3), 5567–5596, doi:10.1029/JD090iD03p05567, 1985.

Langenfelds, R. L., Francey, R. J., Pak, B. C., Steele, L. P., Lloyd, J., Trudinger, C. M., and Allison, C. E., Interannual growth rate variations of atmospheric CO_2 and its $\delta^{13}C$, H_2, CH_4, and CO between 1992 and 1999 linked to biomass burning, Global Biogeochem. Cycles, 16(3), 1048, doi:10.1029/2001GB001466, 2002.

Longden T., Beck, F. J., Jotzo, F., Andrews, R., Prasad, M.,'Clean' hydrogen? – Comparing the emissions and costs of fossil fuel versus renewable electricity based hydrogen, Applied Energy, Volume 306, Part B, 118145, ISSN 0306-2619, doi: 10.1016/j.apenergy.2021.118145, 2022.

Masarie, K. A., Langenfelds, R. L., Allison, C.E., et al., NOAA/CSIRO Flask Air Intercomparison Experiment: A strategy for directly assessing consistency among atmospheric measurements made by independent laboratories, J. Geophys. Res., 106(D17), 20445–20464, doi:10.1029/2000JD000023, 2001.

Montzka, S.A., Dutton, G.S., Yu, P. et al. An unexpected and persistent increase in global emissions of ozone-depleting CFC-11. Nature 557, 413–417, doi: 10.1038/s41586-018-0106-2, 2018.

Novelli, P. C., Elkins, J.W., Steele, L. P., The Development and Evaluation of a Gravimetric Reference Scale For Measurements of Atmospheric Carbon Monoxide, J. Geophys. Res., 96, 13,109-13,121, doi: 10.1029/91JD01108, 1991.

Novelli, P. C., Steele, L. P., and Tans, P. P., Mixing ratios of carbon monoxide in the troposphere, J. Geophys. Res., 97, 20,731-20,750, doi:10.1029/92JD02010, 1992.

Novelli, P. C., Lang, P. M., Masarie, K. A., Hurst, D. F., Myers, R., and W., E. J.: Molecular hydrogen in the troposphere: Global distribution and budget, J. Geophys. Res., 104, 30427–30444, doi: 10.1029/1999JD900788, 1999.

Novelli, P. C., Crotwell, A. M., and Hall, B. D., Application of Gas Chromatography with a Pulsed Discharged Helium Ionization Detector for Measurements of Molecular Hydrogen, Env. Sci. Technol. (43), 2431-2436, doi: 10.1021/es803180g, 2009.

Ocko, I. B. and Hamburg, S. P.: Climate consequences of hydrogen emissions, Atmos. Chem. Phys., 22, 9349–9368, doi: 10.5194/acp-22-9349-2022, 2022.

Oltmans S. J. and Levy, H. II, Surface ozone measurements from a global network, Atmospheric Environment, Volume 28, Issue 1, Pages 9-24, ISSN 1352-2310, doi: 10.1016/1352-2310(94)90019-1, 1994.

Petetin, H., Sauvage, B., Parrington, M., Clark, H., Fontaine, A., Athier, G., Blot, R., Boulanger, D., Cousin, J.-M., Nédélec, P., and Thouret, V.: The role of biomass burning as derived from the tropospheric CO vertical profiles measured by IAGOS aircraft in 2002–2017, Atmos. Chem. Phys., 18, 17277–17306, doi: 10.5194/acp-18-17277-2018, 2018.

Pétron, G., et al., Hydrocarbon emissions characterization in the Colorado Front Range: A pilot study, J. Geophys. Res., 117, D04304, doi:10.1029/2011JD016360, 2012.

Pétron, G., Crotwell, A., Crotwell, M., Kitzis, D., Madronich, M., Mefford, T., Moglia, E., Mund, J., Neff, D., Thoning, K., & Wolter, S., Atmospheric Hydrogen Dry Air Mole Fractions from the NOAA GML Carbon Cycle Cooperative Global Air Sampling Network, 2009-2021 [Data set]. NOAA GML CCGG Division. Version: 2023-05-25, doi: 10.15138/WP0W-EZ08, 2023a.

Pétron G., A.M. Crotwell, M.J. Crotwell, E. Dlugokencky, M. Madronich, E. Moglia, D. Neff, K. Thoning, S. Wolter, J.W. Mund, Atmospheric Carbon Monoxide Dry Air Mole Fractions from the NOAA GML Carbon Cycle Cooperative Global Air Sampling Network, 1988-2022, Version: 2023-08-28, doi: 10.15138/33bv-s284, 2023b.

Price, H., Jaegle, L., Rice, A., Quay, P., Novelli, P. C., and Gammon, R.: Global budget of molecular hydrogen and its deuterium content: Constraints from ground station, cruise, and aircraft observations, J. Geophy. Res., 112, D22108, doi:10.1029/2006JD008152, 2007.

Propper, R., Wong, P., Bui, S., Austin, J., Vance, W., Alvarado, Á., Croes, B., and Luo, D., Ambient and Emission Trends of Toxic Air Contaminants in California, Environmental Science & Technology, 49 (19), 11329-11339, doi: 10.1021/acs.est.5b02766, 2015.

Schultz, M.G., Akimoto, H., Bottenheim, J., et al., The Global Atmosphere Watch reactive gases measurement network. Elementa: Science of the Anthropocene, 3, doi: 10.12952/journal.elementa.000067, 2015.

Simmonds, P. G., Derwent, R. G., O'Doherty, S., Ryall, D. B., Steele, L. P., Langenfelds, R. L., Salameh, P., Wang, H. J., Dimmer, C. H., and Hudson, L. E.: Continuous high-frequency observations of hydrogen at the Mace Head baseline atmospheric monitoring station over the 1994–1998 period, J. Geophys. Res., 105, 12105–12121, doi: 10.1029/2000JD900007, 2000.

Simmonds, P. G., A.J. Manning, R.G. Derwent, P. Ciais, M. Ramonet, V. Kazan, D. Ryall, A burning question. Can recent growth rate anomalies in the greenhouse gases be attributed to large-scale biomass burning events?, Atmospheric Environment, Volume 39, Issue 14,Pages 2513-2517, doi: 10.1016/j.atmosenv.2005.02.018, 2005.

Simpson, I.J., M.P.S. Andersen, S. Meinardi, L. Bruhwiler, N.J. Blake, et al., Long-term decline of global atmospheric ethane concentrations and implications for methane. Nature, 488(7412):490–494, doi: 10.1038/nature11342, 2012.

Steele, L.P., Fraser, P.J., Rasmussen, R.A. et al. The global distribution of methane in the troposphere. J Atmos Chem 5, 125–171, doi: 10.1007/BF00048857, 1987.

Storm, I., Karstens, U., D'Onofrio, C., Vermeulen, A., and Peters, W.: A view of the European carbon flux landscape through the lens of the ICOS atmospheric observation network, Atmos. Chem. Phys., 23, 4993–5008, doi: 10.5194/acp-23-4993-2023, 2023.

Tans, P.P., Thoning, K.W., Elliot, W.P., and Conway, T.J., *Background atmospheric CO_2 patterns from weekly flask samples at Barrow, Alaska: Optimal signal recovery and error estimates,* NOAA Tech. Memo. (ERL-ARL-173). Environ. Res. Lab., Boulder, Colo., 131 pp. 1989a.

Tans, P.P., T.J. Conway, and T. Nakazawa, Latitudinal distribution of the sources and sinks of atmospheric carbon dioxide derived from surface observations and an atmospheric transport model, J. Geophys. Res., 94, 5151-5172, doi: 10.1029/JD094iD04p05151, 1989b.

Thompson A. M., J. C. Witte, S. J. Oltmans, F. J. Schmidlin, SHADOZ - A tropical ozonesonde-radiosonde network for the atmospheric community. Bulletin of the American Meteorological Society, Vol. 85, No. 10, pp. 1549-1564, http://www.jstor.org/stable/26221206, 2004.

Thoning, K.W., P.P. Tans, and W.D. Komhyr, Atmospheric carbon dioxide at Mauna Loa Observatory 2. Analysis of the NOAA GMCC data, 1974-1985, J. Geophys. Res., 94, 8549-8565, doi: 10.1029/JD094iD06p08549, 1989.

Tørseth, K., Aas, W., Breivik, K., Fjæraa, A. M., Fiebig, M., Hjellbrekke, A. G., Lund Myhre, C., Solberg, S., and Yttri, K. E.: Introduction to the European Monitoring and Evaluation Programme (EMEP) and observed atmospheric composition change during 1972–2009, Atmos. Chem. Phys., 12, 5447–5481, doi: 10.5194/acp-12-5447-2012, 2012.

van der Velde, I.R., van der Werf, G.R., Houweling, S. *et al.* Vast CO2 release from Australian fires in 2019–2020 constrained by satellite. *Nature* 597, 366–369, doi: 10.1038/s41586-021-03712-y, 2021.

von Schneidemesser E., Monks, P.S., Plass-Duelmer C., Global comparison of VOC and CO observations in urban areas, Atmospheric Environment, Volume 44, Issue 39,Pages 5053-5064, ISSN 1352-2310, doi: 10.1016/j.atmosenv.2010.09.010, 2010.

Yver, C. E., Pison, I. C., Fortems-Cheiney, A., A new estimation of the recent tropospheric molecular hydrogen budget using atmospheric observations and variational inversion, Atmos. Chem. Phys., 11, 3375–3392, doi: 10.5194/acp-11-3375-2011, 2011.

Warwick, N., Griffiths, P., Keeble, J., Archibald A., Pyle, J., and Shine, K.: Atmospheric implications of increased Hydrogen use, UK government's Department of Business, Energy and Industrial Strategy (BEIS) report, 2022. Accessible at: https://assets.publishing.service.gov.uk/media/624eca7fe90e0729f4400b99/atmospheric-implications-of-increased-hydrogen-use.pdf, Last accessed: October 18, 2023.

Warwick, N. J., Archibald, A. T., Griffiths, P. T., Keeble, J., O'Connor, F. M., Pyle, J. A., and Shine, K. P.: Atmospheric composition and climate impacts of a future hydrogen economy, Atmos. Chem. Phys., 23, 13451–13467, https://doi.org/10.5194/acp-23-13451-2023, 2023.

World Meteorological Organization, Global Atmospheric Watch, 20th WMO/IAEA Meeting on Carbon Dioxide, Other Greenhouse Gases and Related Measurement Techniques (GGMT-2019), report 255, 2020. Accessible at: https://library.wmo.int/records/item/57135-20th-wmo-iaea-meeting-on-carbon-dioxide-other-greenhouse-gases-and-related-measurement-techniques-ggmt-2019. Last accessed: December 4, 2023.

World Meteorological Organization, Greenhouse Gas Bulletin (18): The State of Greenhouse Gases in the Atmosphere Based on Global Observations through 2021. 10p., 2022. Accessible at: https://library.wmo.int/idurl/4/58743. Last accessed: January 2, 2024.

Worthy, D. E. J., Rauh, M. K., Huang, L., et al.,Results of a Long-Term International Comparison of Greenhouse Gas and Isotope Measurements at the Global Atmosphere Watch (GAW) Observatory in Alert, Nunavut, Canada, Atmos. Meas. Tech., 16, 5909–5935, doi: 10.5194/amt-16-5909-2023, 2023.

Yap, J., and McLellan B. A., Historical Analysis of Hydrogen Economy Research, Development, and Expectations, 1972 to 2020, Environments, *10*, 11, doi: 10.3390/environments10010011, 2023.

Zheng, B., Ciais, P., Chevallier, F., et al., Record-high CO_2 emissions from boreal fires in 2021. Science, 379, 912-917, doi: 10.1126/science.ade0805, 2023.

Tables

Table 1. NOAA GML H_2 primary standards (prepared gravimetrically) and their WMO/MPI X2009 assignments (dated 2022-02-18). All H_2 dry air mole fractions and their uncertainties are in ppb.

Serial Number	Fill code	Fill Date	CCL value	CCL uncertainty
SX-3558	A	2008-10-17	248.4	0.1
SX-0614470	A	2019-04-15	352.8	0.1
SX-3543	B	2008-11-03	425.4	0.2
SX-3540	B	2007-08-07	488	0.2
SX-0614471	A	2019-04-19	496.5	0.3
SX-3523	C	2007-07-24	527	0.2
SX-3554	A	2007-08-02	601.2	0.2
SX-0614472	A	2019-04-19	701.9	0.2

~~Table 2: H_2 secondary standards used in the tank calibration laboratory and H_2 tertiary standards used on the MAGICC-1 and MAGICC-2 systems (2009 to 2019).~~

~~Tank Calibration / H9~~								
~~Tank ID (fill)~~	~~Time of use~~	~~t0~~	~~Assignment at t0 (ppb)~~	~~C1 (ppb/yr)~~	~~C2 (ppb/yr^2)~~	~~N~~	~~Residuals standard deviation (ppb)~~	~~Fill date~~
~~CC119811 (A)~~	~~2/05/2008 to 6/02/2013~~	~~2010.0689~~	~~549.4~~	~~2.0~~	~~0~~	~~47~~	~~0.50~~	~~01/01/2006 SM*~~
~~CA03233 (B)~~	~~6/02/2013 to 11/01/2018~~	~~2016.7106~~	~~502.8~~	~~0~~	~~0~~	~~19~~	~~0.23~~	~~08/12/2010 NWR~~
~~MAGICC-1 / H11~~								
~~Tank ID (fill)~~	~~Time of use~~	~~t0~~	~~Assignment at t0 (ppb)~~	~~C1 (ppb/yr)~~	~~C2 (ppb/yr^2)~~	~~N~~	~~Assignment uncertainty (ppb)**~~	~~Fill date~~
~~CA08107 (D)~~	~~7/22 to 8/7/2019~~	~~2019.2959~~	~~562.9~~	~~15.4~~	~~0~~	~~6~~	~~0.6~~	~~11/9/2018 NWR~~
~~CB11090 (B)~~	~~10/18/2018 to 7/19/2019~~	~~2019.1482~~	~~576.3~~	~~6.9~~	~~0~~	~~4a~~	~~0.6 After 2019-06-21: 1.5~~	~~9/30/2016 NWR~~
~~CB11551 (A)~~	~~2/13 to 10/17/2018~~	~~2018.1878~~	~~548.8~~	~~6.7~~	~~0~~	~~3a,b, c~~	~~0.5 After 2018-08-27: 1.5~~	~~1/1/2015 SM*~~
~~CC91285 (C)~~	~~6/19/2017 to 2/13/2018~~	~~2017.1711~~	~~538.4~~	~~0~~	~~0~~	~~8~~	~~0.5~~	~~8/14/2015 NWR~~
~~CA08165~~	~~10/13/2016 to~~	~~2016.9137~~	~~535.7~~	~~4.5~~	~~0~~	~~3c~~	~~0.5~~	~~12/16/2011~~

(B)	06/16/2017							NWR
CC302566 (B)	3/21/2016 to 10/12/2016	2016.3645	540.2	4.4	0	5	0.5	8/14/2015 NWR
CC105491 (B)	8/10/2015 to 3/18/2016	2015.1506	522.3	0	0	5d	1.0	1/16/2014 NWR
ND33801 (B)	8/4/2014 to 8/7/2015	2013.8771	509.3	0.9	0	6e	0.5 After 2015-05-14: 1.0	12/27/2012 NWR
CB09117 (A)	2/18 to 8/1/ 2014	2013.8912	635.3	28.7	0	5	2	12/17/2012 SM
ND46735 (A)	9/10/2012 to 2/13/2014	2012.9158	527.4	2.5	-1.0	7e,f	0.5 After 2013-12-11: 1.0	1/1/2011 estimated
CA04505 (B)	12/9/2011 to 9/7/2012	2011.4593	540.6	1.7	0	3c,d	1.0	8/12/2010 NWR
ND38963 (A)	8/12/2010 to 12/7/2011	2011.704	586.0	6.2	0	4	0.5	1/1/2009 estimated
CC71649 (E)	1/22 to 8/6 2010	2009.1184	507.1	8.4	0	7b,e	1.5	9/19/2008
MAGICC-2 / H8								
Tank ID (fill)	Time of use		Assignment at t0 (ppb)	C1	C2	N	Assignment uncertainty (ppb)**	Fill date
ND38954 (B)	3/26/2013 to 3/21/2014	2014.2094	516.6	2.0	0	5	0.5	12/9/2012 NWR
CA03409 (B)	5/23/2011 to 3/25/2013	2011.6278	526.6	0	0	5e	0.5 After 2013-01-21: 1.0	1/1/2010 estimated
ND38415 (A)	4/5/2010 to 5/20/2011	2010.2502	566.1	20.9	-8.7	6	0.5	1/1/2009 estimated
CC305198 (A)	11/2//2009 to 4/3/2010	2009.7211	557.9	65.8	0	3a,b	1.5 After 2010-01-31: 2.5	1/1/2009 SM*

* Gravimetric blends with CO, H_2, CO_2, CH_4 and N_2O in zero air purchases from Scott Marrin.

** Uncertainty estimates listed for the tertiary standard assignments assume a 0.5 ppb uncertainty for each calibration result on H9 and do not formally include the uncertainty on the secondary standard assignments.

a. Assignment does not use existing post-use calibration results that show larger drift
b. Drift change towards end of use, additional drift correction applied.
c. Force linear fit in drift calculation code
d. Only predeployment calibrations
e. No end-of-use or post-use calibration
f. Force quadratic fit in drift calculation code

Table 3: H_2 working standards used on the MAGICC-3 system. Best polynomial curve fit coefficients to the August 2019-December 2022 calibration histories.

Tank ID (fill)	t0	Assignment at t0 (ppb)	C1 (ppb/yr)	C2 (ppb/yr^2)	N	Assignment uncertainty (ppb)	Fill date
CA01414 (I)	2020.0964	238.4	10.0	-1.9	9	0.5 ppb	12/29/2017 NWR
CA04403 (F)	2020.1052	474.6	10.2	-1.7	9	0.5 ppb	12/1/2017 NWR
CB11270 (A)	2020.0012	515.0	2.9	-0.5	9	0.5 ppb	12/1/2017 NWR
CA06388 (H)	2019.9423	551.2	1.1	0	9	0.5 ppb	2/23/2018 NWR
CA05773 (F)	2020.2585	565.6	1.4	0	8	0.5 ppb	5/17/2018 NWR
CB11034 (B)	2020.0783	580.1	8.3	-1.2	9	0.5 ppb	5/17/2018 NWR
CA05680 (H)	2020.0904	588.1	1.9	0	9	0.5 ppb	12/1/2017 NWR
CB11405 (C)	2020.1474	605.6	23.3	-1.6	9	0.5 ppb	5/17/2018 NWR

Table 24: H9 Target air tanks with zero or linear growth in H_2

Linear Drift Rate (ppb/yr)	Target Tank IDs	Standard deviation of residuals to best fits (ppb)
0	CA05278, CA06194, CA08247, CC121971, CC311842 ND16439, ND33960	0.46
0-1	ALM-065166, CA05300, CC71607, CC73110	0.42
2-5	CA04551, CA07328, CB10910	0.32
5-10	CC71579	0.36
> 20	CA08145	0.48

Table 35. Summary statistics for H_2 differences between test air tank-fill assignment (based on H9 calibration history) and associated TST flask measurements on MAGICC systems

System / Instrument	Test air tank id and fill	Differences mean (ppb)	Differences standard deviation (ppb)	Number of samples
MAGICC-2 / H8	AL43-113 D, E	-0.3	1.3	528
MAGICC-1 / H11	AL43-113 D, E, G	+0.3	1.1	1231
MAGICC-3 / H8	AL47-145 G	-0.9	1.5	388
MAGICC-3 / H11	AL43-113 G	+0.4	0.6	144

Table 6. Summary statistics for SPO flask pair H_2 differences. Npairs= Number of flask pairs.

System/ Instrument	SPO "P" flasks Absolute differences			SPO "S" flasks Absolute differences			SPO "S"-"P" Pair mean differences		
	Mean (ppb)	Std dev (ppb)	Npairs	Mean (ppb)	Std dev (ppb)	Npairs	Mean (ppb)	Std dev (ppb)	Npairs
MAGICC-2 / H8	1.3	1.0	165	1.1	0.9	87	-0.4	1.5	81
MAGICC-1 / H11	0.9	0.8	292	0.9	0.8	143	-0.2	1.3	144
MAGICC-3 / H8	1.6	1.3	45	1.2	1.2	25	-0.1	1.7	25
MAGICC-3 / H11	0.7	0.6	76	0.8	0.6	35	-0.5	0.8	43

Table 4: Flask air H_2 measurement uncertainty components

Uncertainty components	1 sigma uncertainty estimate (ppb)	Source
Tertiary standard time-dependent assignment uncertainty (1 point calibration)	0.5-2.5 Tank specific (see SI Table 2)	Calibration histories, residuals to best fit, TST flasks
MAGICC-3 response curve uncertainty	0.5	Preliminary estimate, will be reassessed.
Measurement repeatability on H8	1.3 (MAGICC-2) 1.5 (MAGICC-3)	TST and SPO flask pair differences (Table 3 and SI Table 6)
Measurement repeatability on H11	1.1 (MAGICC-1) 0.6 (MAGICC-3)	

Table 5~~7~~: Annual mean of H_2 measurement differences (in ppb) for air samples from the Cape Grim Observatory (CGO), Ochsenkopf (OXK) and Alert (ALT). Non background air sample measurement results are included. Col~~l~~ocated (not same air) samples at ALT are matched within a +/- 60 minutes window. ~~[updated 9-25-23]~~

Year	NOAA ICP-NOAA nonICP		CGO NOAA non ICP minus CSIRO ICP	OXK NOAA ICP minus MPI ICP	ALT NOAA minus CSIRO (not same air)	ALT NOAA minus MPI (not same air)
	CGO*	OXK				
2010	-	-0.05	0.72	-0.17	-3.4	-3.5
2011	-	0.15	0.50	-0.02	2.2	-3.9
2012	0.58	0.13	0.40	-0.29	0.66	-2.3
2013	-	0.01	0.23	0.80	1.30	-1.4
2014	-	0.19	1.37	1.61	0.63	-1.1
2015	-	0.85	0.02	0.53	0.52	-1.4
2016	1.32	0.20	1.54	2.91	-0.32	-1.4
2017	1.19	0.56	1.38	2.49	3.2	-
2018	0.91	0.53	1.31	1.69	1.2	-1.3
2019	0.73	-0.07	0.30	1.25	1.0	-0.81
2020	0.18	na	0.19	-	0.01	-0.22
2021	0.33	0.33	0.86	1.71	3.4	-

*Most NOAA ICP flasks from CGO had a small contamination for CO and H_2 prior to 2019. If the NOAA ICP flask H_2 results are > 2ppb larger than the NOAA non-ICP flask H_2 in the pair, the ICP flask H_2 has been rejected. Only years with at least 10 valid H_2 pairs are included.

Table 78: Flask air H_2 measurement uncertainty components

Uncertainty components	1 sigma uncertainty estimate (ppb)	Source
Tertiary standard time-dependent assignment uncertainty (1 point calibration)	0.5-2.5 Tank specific (see Table 2)	Calibration histories, residuals to best fit, TST flasks
MAGICC-3 response curve uncertainty	0.5	Preliminary estimate, will be reassessed.
Measurement repeatability on H8	1.3 (MAGICC-2) 1.5 (MAGICC-3)	TST and SPO flask pair differences (Tables 5 and 6)
Measurement repeatability on H11	1.1 (MAGICC-1) 0.6 (MAGICC-3)	

Figures

Figure 1. Calibration results for GML two H_2 secondary standards (a) CC119811 and b) CA03233) on H9 against one of the primary standards. 2019-2020 multipoint calibration results on H9 are also shown for CA03233 (pink circles). Only results shown with open circles are used for the assignments.

Figure 2: 2019-2022 H9 standard calibration response curve (RC) results: a) differences from the mean RC linear fit ~~mean~~ and b) residuals of the response curve fits. Different colors are for different calibration episodes.

Figure 3. Calibration histories of a) MAGICC-1 / H11 and b) MAGICC-2 / H8 tertiary standards. The colored vertical line indicates when a standard started to be used.

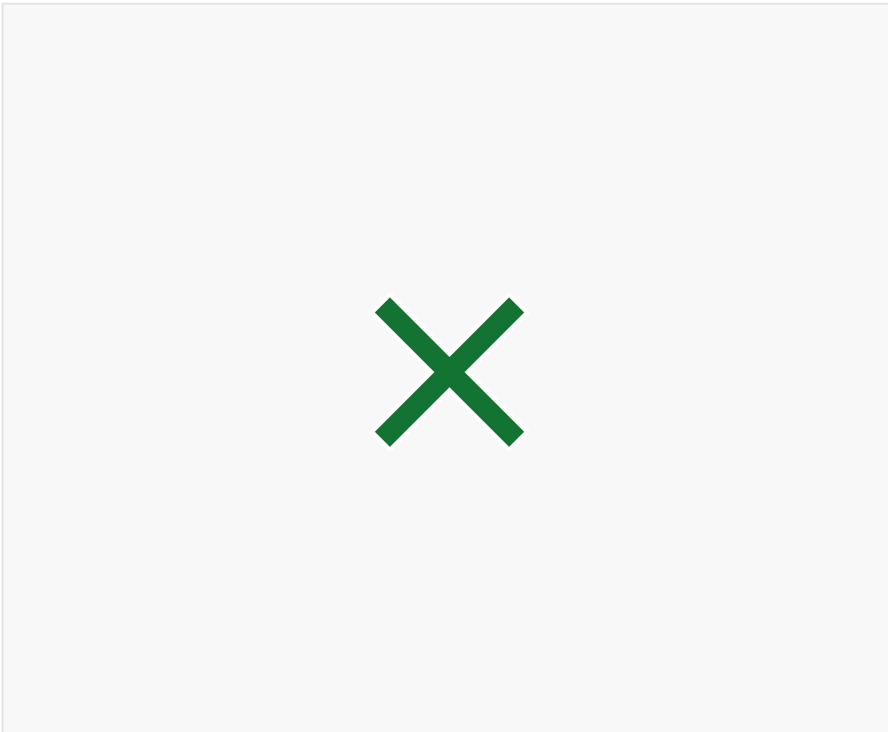

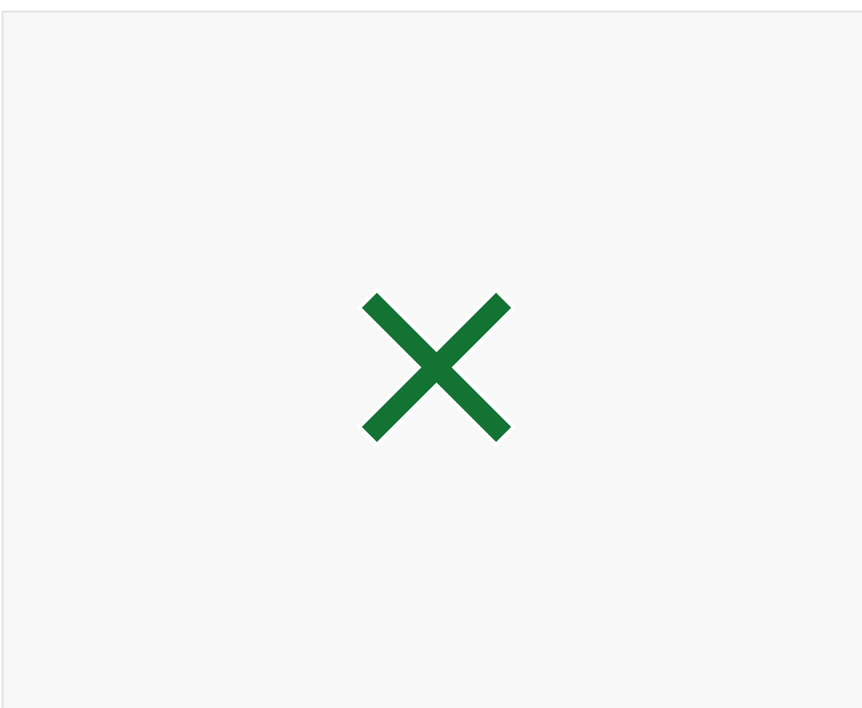

Figure 4: Calibration histories and residuals to best fit for H9 target tanks with a stable H_2 mole fraction or a linear drift less than 1 ppb/yr. Residuals are in ppb.

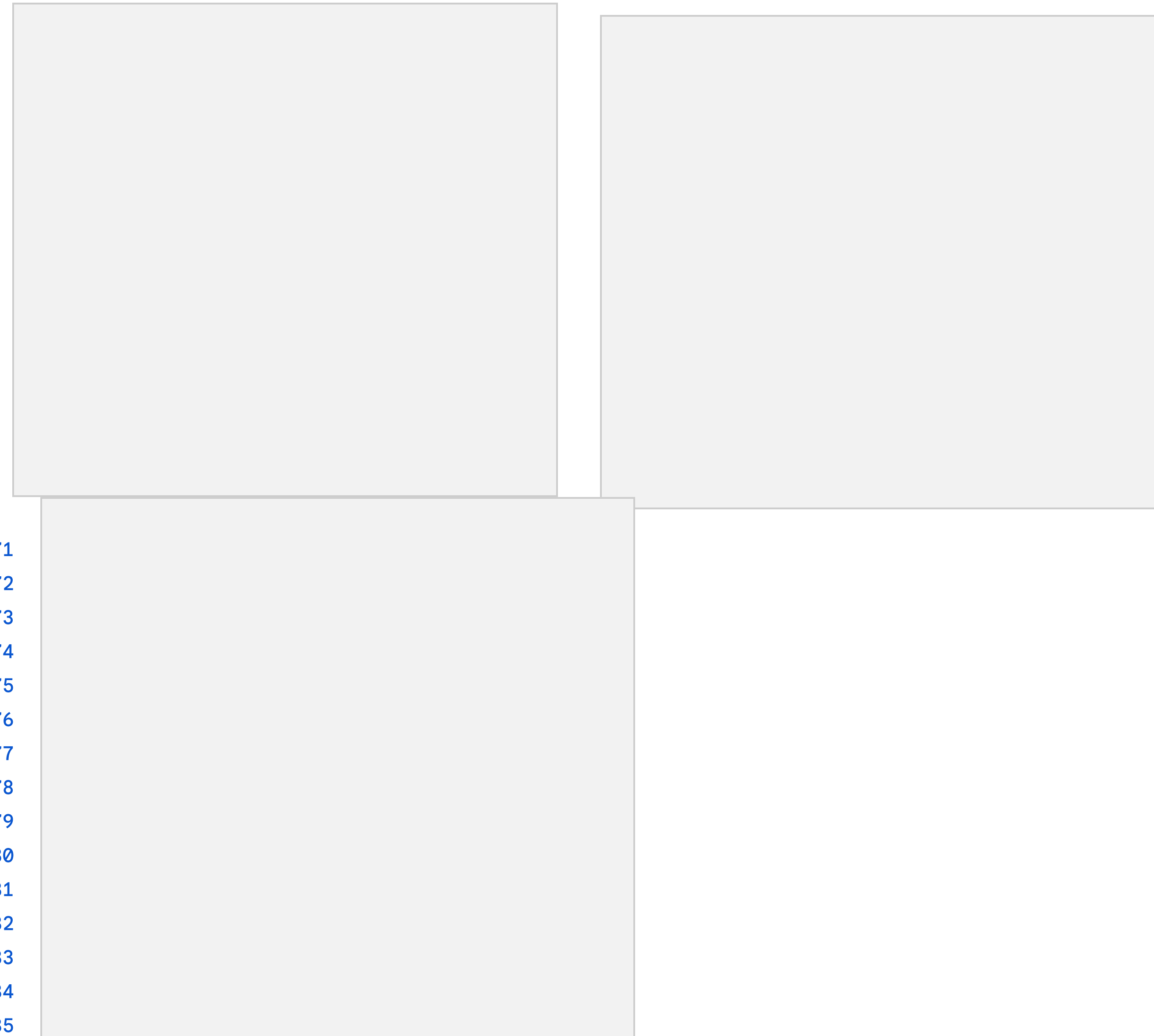

Figure 5. Flask air analysis systems ~~(H8 and H11)~~ target air tanks H9 a) calibration histories and b) residuals to best linear or quadratic fit.

Figure 6. Differences of target air tank H_2 analysis results on a) H11 and b) H8~~MAGICC~~ and the time-dependent assignment based on calibration history on H9. ~~The vertical line indicates the transition to the MAGICC-3 flask analysis system.~~

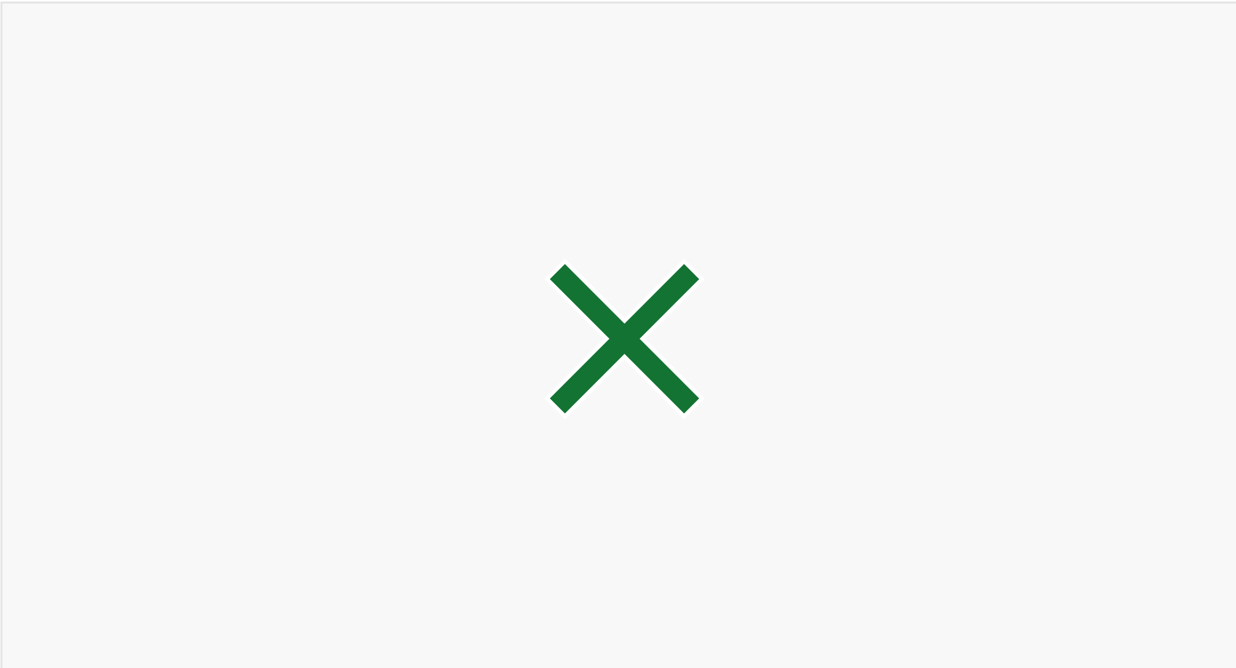

Figure 7. South Pole Observatory flask air H_2 measurements on H11 and H8. Black symbols are used for measurements of P flasks and blue symbols are used for measurements of S flasks.

Figure 7. South Pole Observatory flask air H_2 measurements. Circle and "+" symbols refer to instruments: H11 or H8. Black is used for measurements of P flasks on the MAGICC-1 or MAGICC-2 system and red for the MAGICC-3 system. Light green is used for measurements of S flasks on the MAGICC-1 or MAGICC-2 system and light blue for the MAGICC-3 system. ¶

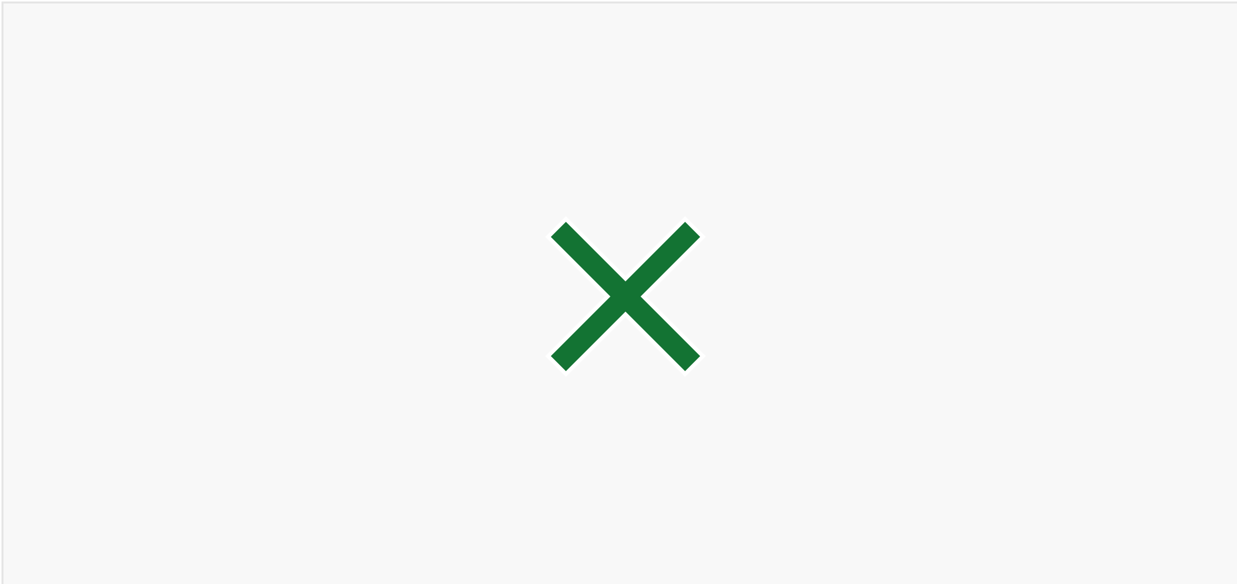

Figure 8. Interlaboratory same air H_2 measurement difference for OXK ICP (NOAA - MPI-BGC) and CGO (NOAA non ICP - CSIRO ICP).

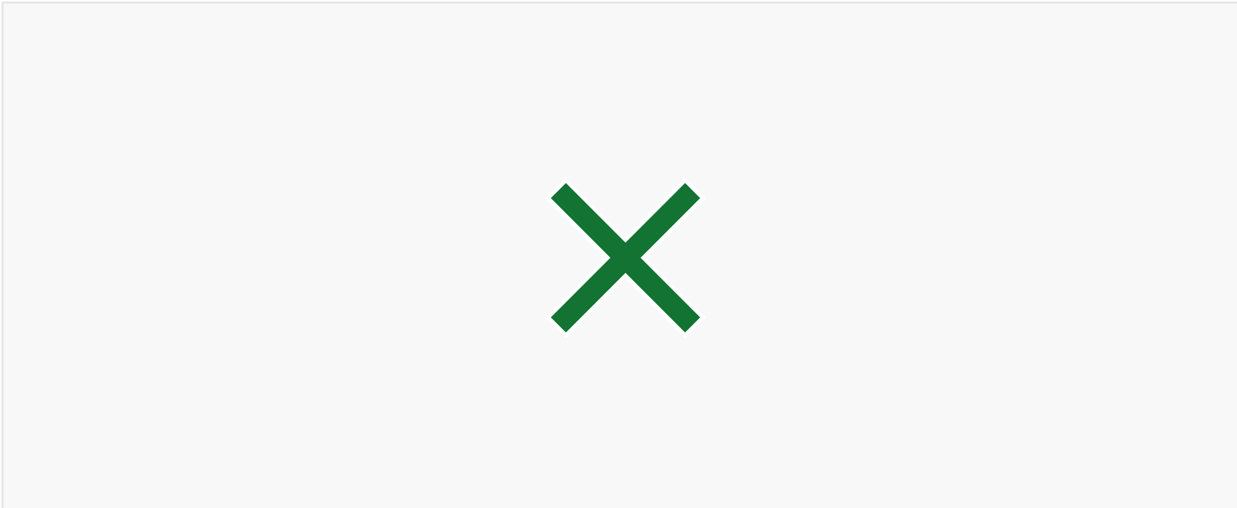

Figure 9~~10~~: Annual maximum (red), mean (green) and minimum (blue) H_2 from the smooth curve fit of the 2010-2021 measurement time series for each surface site in the global sampling network. Each site is referred to with a three letter code (see details in SI Table 7~~at https://gml.noaa.gov/dv/site/~~). The sampling sites are shown along the x-axis with decreasing latitudes. An asterisk near the site code indicates if the site data are~~is~~ used for the marine boundary layer air zonal and global means H_2 data reduction.

Figure 109. H_2 time series at the NOAA Baseline Atmospheric Observatories

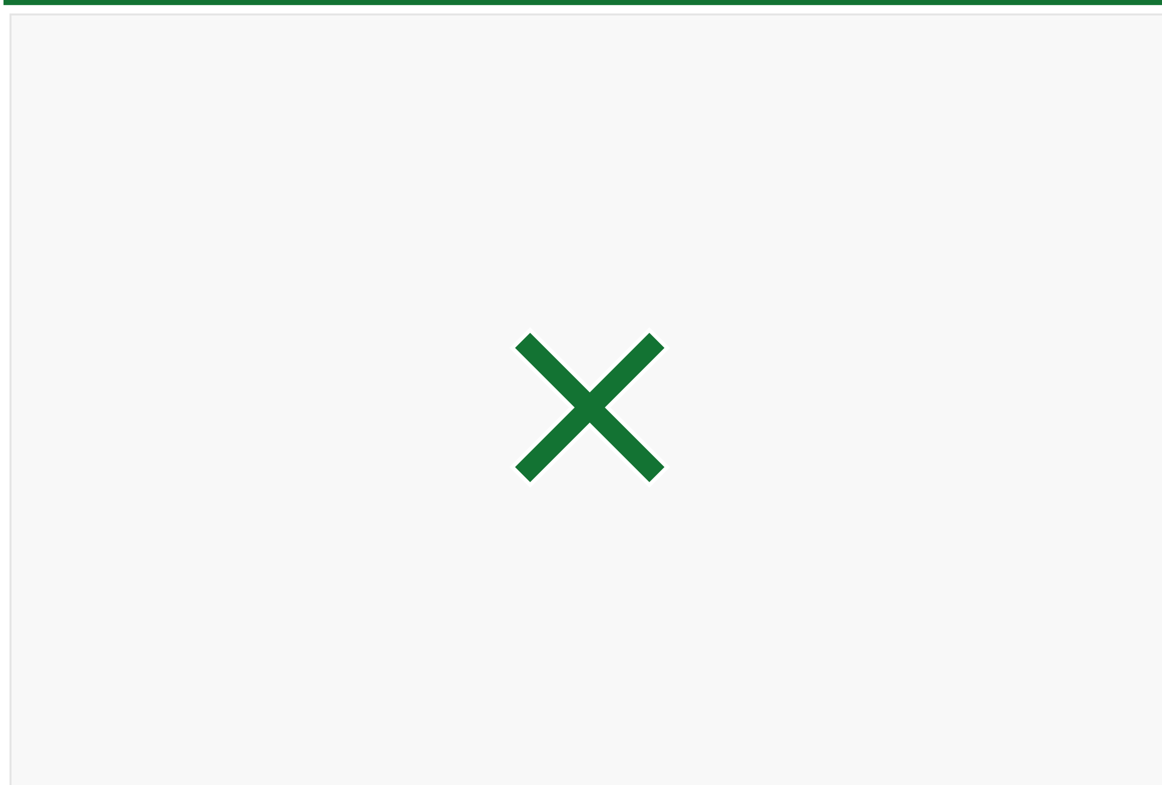

Figure 11: 2010-2021 marine boundary layer H_2 meridional gradient. Y-axis is the sine of latitude.

Figure 12: 2010-2021 marine boundary layer global mean and zonal mean H_2 anomaly (black line) and CO anomaly (dashed blue line) time series.